

# Paleoceanography and Paleoclimatology

## RESEARCH ARTICLE

10.1029/2018PA003553

### Key Points:

- Age offsets cannot be predicted from estimates of sedimentation rate and the thickness of the surface mixed layer (SML)
- Where bioturbation extends below the surficial taphonomic active zone with high shell loss, old shells will be admixed with young shells
- Between-species differences in the history of shell production magnify between-species age offsets

### Supporting Information:

- Supporting Information S1
- Table S1
- Table S2
- Table S3
- Table S4
- Table S5

### Correspondence to:

A. Tomašových,  
geoltoma@savba.sk

### Citation:

Tomašových, A., Kidwell, S. M., Alexander, C. R., & Kaufman, D. S. (2019). Millennial-scale age offsets within fossil assemblages: Result of bioturbation below the taphonomic active zone and out-of-phase production. *Paleoceanography and Paleoclimatology*, 34, 954–977. <https://doi.org/10.1029/2018PA003553>

Received 2 JAN 2019

Accepted 6 MAY 2019

Accepted article online 12 MAY 2019

Published online 23 JUN 2019

Corrected 12 JUL 2019

This article was corrected on 12 JUL 2019. See the end of the full text for details.

©2019. American Geophysical Union.  
All Rights Reserved.

## Millennial-Scale Age Offsets Within Fossil Assemblages: Result of Bioturbation Below the Taphonomic Active Zone and Out-of-Phase Production

A. Tomašových<sup>1</sup> , S. M. Kidwell<sup>2</sup>, C. R. Alexander<sup>3</sup>, and D. S. Kaufman<sup>4</sup>

<sup>1</sup>Earth Science Institute, Slovak Academy of Sciences, Bratislava, Slovakia, <sup>2</sup>Department of Geophysical Sciences, University of Chicago, Chicago, IL, USA, <sup>3</sup>Skidaway Institute of Oceanography, University of Georgia, Savannah, GA, USA, <sup>4</sup>School of Earth and Environmental Sustainability, Northern Arizona University, Flagstaff, AZ, USA

**Abstract** Oceanographic and evolutionary inferences based on fossil assemblages can be obscured by age offsets among co-occurring shells (i.e., time averaging). To identify the contributions of sedimentation, mixing, durability, and production to within- and between-species age offsets, we analyze downcore changes in the age-frequency distributions of two bivalves on the California shelf. Within-species age offsets are ~50–2,000 years for *Parvilucina* and ~2,000–4,000 years for *Nuculana* and between-species offsets are 1,000–4,000 years within the 10- to 25-cm-thick stratigraphic units. Shells within the top 20–24 cm of the seabed are age-homogeneous, defining the thickness of the surface completely-mixed layer (SML), and have strongly right-skewed age-frequency distributions, indicating fast shell disintegration. The SML thus coincides with the taphonomic active zone and extends below the redoxcline at ~10 cm. Shells >2,000–3,000 years old occurring within the SML have been exhumed from subsurface shell-rich units rich where disintegration is negligible (sequestration zone, SZ). Burrowers (callianassid shrimps) penetrate 40–50 cm below the seafloor into this SZ. The millennial offsets within each increment result from the advection of old shells from the SZ, combined with an out-of-phase change in species production. Age unmixing reveals that *Parvilucina* was abundant during the transgressive phase, rare during the highstand phase, and increased steeply in the twentieth century in response to wastewater. *Nuculana* was abundant during the highstand phase and has declined over the past two centuries. This sequestration-exhumation dynamic accentuates age offsets by allowing both the persistence of shells below the SML and their later admixing with younger shells within the SML.

## 1. Introduction

Continental shelf sediments are valuable archives of oceanographic and biological history that allow inferences about the timing and causes of changes in climate, productivity, and seawater chemistry (Birks & Koç, 2002; Keigwin & Jones, 1995; Knies et al., 2003; Kobashi et al., 2004) and about evolutionary and ecological dynamics (e.g., Myhre et al., 2017; O'Dea et al., 2007; Pandolfi, 1996). However, as in pelagic sediments, bioturbational mixing by diffusion or advection increases time averaging (i.e., age offsets among co-occurring individuals and species) of fossil assemblages and can alter the distribution of species in stratigraphic successions, thereby modifying community composition, co-occurrence patterns, patterns of first and last appearances, and turnover rates (Alegret et al., 2015; Anderson et al., 1997; Lazarus et al., 2012; MacLeod & Huber, 1996; Nawrot et al., 2018; Tomašových & Kidwell, 2010). The time averaging of fossil assemblages is commonly approximated by dividing the thickness of the mixed layer by sedimentation rate (Anderson, 2001; Wheatcroft, 1990) and thus depends on the simultaneous estimation of (a) sedimentation rate and (b) depth of sediment mixing by bioturbation (Bentley et al., 2006; Bentley & Nittrouer, 2003; Wheatcroft & Drake, 2003; Wit et al., 2013).

In practice, however, estimating sedimentation and mixing parameters is difficult. First, bioturbational mixing complicates the use of tracers for estimates of sedimentation rate (Johannessen & Macdonald, 2012; Keigwin & Guilderson, 2009); second, temporal variability in tracer production can obscure estimates of both mixing (depth of mixing and biodiffusion coefficient) and sedimentation rate (Broecker et al., 1999; Guinasso & Schink, 1975; Johannessen & Macdonald, 2012; Kemp & Sexton, 2014); and third, the depth of sediment mixing by bioturbation is not simply equal to the depth of the completely-mixed layer (Teal et al., 2008; Uchman & Wetzel, 2011). For example, using mollusk shells as a dateable tracer with

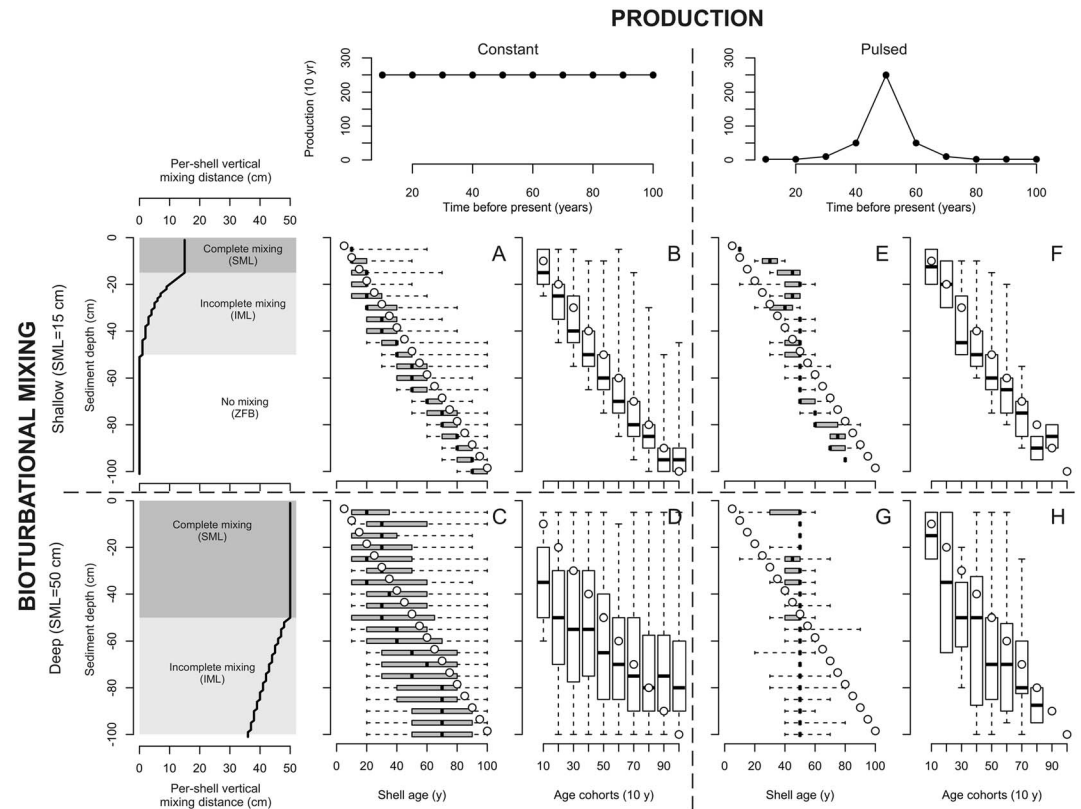


**Figure 1.** Effects of complete (surface completely-mixed layer) and incomplete mixing (e.g., discrete burrows of non-local feeders such as callianassids), extending over two depths (top and bottom rows) and interacting with either constant (a–d) or pulsed (e–h) shell production, assuming sedimentation (shell-burial) rate = 1 cm/year and no postmortem loss of shells, using 100-cm-long cores and the modeling approach of Olszewski (2004, Text S1). The model assumes that the probability that a shell will be moved vertically per time step decreases with sediment depth, generating three layers with complete mixing (SML), incomplete mixing (IML), and no active mixing (i.e., zone of final burial). Downcore changes in the apparent age of increments (a, c and e, g; gray boxplots denote median age and 25th and 75th age quantiles) reflect the expected depth distribution of 10-year age cohorts of shells (b, d, f, and h; white boxplots denote median depth and 25th and 75th depth quantiles) as a function of shallow (SML = 15 cm) and deep complete mixing (SML = 50 cm). White circles denote increment ages and sediment depths of age cohorts expected in the absence of mixing. First, under constant shell production (a–d, left graphs), age profiles are homogeneous over 15 cm (a) or 40–50 cm (c) as predicted by the SML thickness. Age profiles below the SML are slightly steeper than expected in the absence of mixing, but the effects of *incomplete* mixing (that reaches through the entire 100-cm core in the scenario with a deep SML) cannot be detected on the basis of such profiles alone: age profiles are not homogeneous. This situation contrasts with the depth distributions of shell age cohorts: incomplete mixing pulls old shells upward toward the SML, and where mixing is deep, old shells can span the thickness of the whole core (d), revealing that most of the core is indeed affected by mixing. Second, given a pulse in production (right columns) and a shallow SML (e), age profiles are much steeper (shell burial rates are ~2 cm/year) and the *apparent* age homogeneity is increased (i.e., median age remains constant over >50 cm), similar to the profile generated under constant production and a deep SML (c). The sediment depths of age cohorts remain segregated under a shallow SML (b and f)—that is, downcore ordering is preserved—in contrast to scenarios with a deep SML (d and h). Third, pulsed production leads to age overestimation in the upper part of the core and age underestimation in the lower part of the core (e, g). Between-species age offsets can thus be generated if two species have significantly different production trajectories, that is, significantly different timing or magnitude of pulses, and those age offsets will be larger under a deeper SML. The uptick in age cohorts in the last interval is caused by the small number of shells.

potential for temporal variation in production, a simple model assuming constant production and assuming that vertical distance of individual shells moved by burrowers per time step decreases with sediment depth (source code in R language in supporting information Text S1, Meysman et al., 2010; Schiffers et al., 2011; Trauth, 1998) finds that mixing inevitably steepens the downcore profile of shell ages. This steepening leads to the overestimation of sedimentation rate (dashed lines versus open circles, which describe increment age in the absence of mixing; Figures 1a, 1c, 1e, and 1g). However, the depth of mixing itself can be (1) underestimated if focused on age-homogeneous, completely mixed increments without

accounting for incomplete mixing of deeper increments (e.g., by deeply burrowing non-local feeders such as callianassid shrimp; Figures 1a and 1c). The depth of mixing can alternatively be (2) overestimated if age-homogeneous profiles are generated by temporally variable production of shells (Figures 1e and 1g; e.g., median increment ages in Figure 1e are age-homogeneous over 50 cm even though complete mixing acted over only 15 cm, as shown in the left panel). Mixing coupled with variable production can thus both overestimate and underestimate the age of a sedimentary increment depending on whether production increased or decreased toward the Recent (Figures 1e and 1g). The shell age distributions further depend on the magnitude and depth dependence of shell disintegration, which is set to 0 in Figure 1 but is generally assumed to decline with depth.

Existing deconvolution models that extract prebioturbation signatures of ecological, geochemical, or mineralogical records (Bard et al., 1987; Hull et al., 2011; Manighetti et al., 1995; Schiffelbein, 1985; Shull, 2001; Steiner et al., 2016) assume that bioturbation can be modeled by simple diffusion-advection mechanisms. However, first, the ability of pulsed production to produce age homogeneity in a profile (e.g., Figures 1e–1h) confounds the estimates of diffusion and advection used in modeling. Second, the applicability of simple diffusive-advection models of mixing is limited in settings where subsurface increments have been incompletely mixed by non-local feeders, recognizable from their discrete burrows observed on many shelves and within coastal water bodies. This conceptual complexity translates into a three-layer subdivision of sediments on the basis of depth and frequency of burrowing events (Berger et al., 1979), rather than the more conventional subdivision of sediments into a mixed and an unmixed layer. These three layers are the following: the surface completely-mixed layer (SML), typically dominated by bi-diffusion; the incompletely-mixed layer (IML), inhabited by deeper infauna, whose lower boundary is effectively the maximum burrowing depth (referred to as the transition layer in analyses of bioturbation fabric; Bentley & Nittrouer, 2012; Ekdale et al., 1984; Löwemark, 2007; Savrda et al., 1991); and a layer with no active mixing, representing the zone of final burial (Olszewski, 2004). This stratification is sensitive to the timescale over which mixing is measured (Maire et al., 2008; Smith et al., 1993). When measuring the effect of mixing on the temporal resolution of fossil assemblages, this timescale should correspond to the timescale of shell final burial (i.e., the elapsed time to entering the zone of final burial). Increment-specific age-frequency distributions (AFDs) of shells (e.g., Kosnik et al., 2007, 2015; Olszewski & Kaufman, 2015; Tomašových et al., 2014) can reveal the depths of complete and incomplete mixing at such timescales and can directly unmix stratigraphic signals, without any assumptions about the depth or frequency of shell mixing (Tomašových & Kidwell, 2017). AFDs from successive, downcore increments can thus resolve the effects of incomplete mixing both on the temporal resolution of oceanographic and biological data and on the existence of age-homogeneous intervals within a sedimentary core (Tomašových et al., 2017, 2018) and can be informative about the conditions that promote significant age offsets within and between co-occurring species (Kosnik et al., 2009; Scarponi et al., 2013; Tomašových et al., 2016).

Several mechanisms can explain between-species age offsets (Barker et al., 2007; Mekik, 2014; Paull et al., 1991), including (1) temporal differences in species production occurring under very low sedimentation and/or high sediment mixing by bioturbation, leading to age offsets that exceed the duration over which species change in abundance (Ausín et al., 2019; Bard, 2001; Broecker et al., 1999; Loubere, 1989; Löwemark & Grootes, 2004; Manighetti et al., 1995; Peng & Broecker, 1984), and/or (2) differences in disintegration between fragile and robust species, paralleling age mismatches between  $^{210}\text{Pb}$  and  $^{14}\text{C}$  tracers (Barker et al., 2007; Broecker et al., 1991; Broecker & Clark, 2011; DuBois & Prell, 1988; Peng et al., 1979). Mixing and disintegration rates, both integral in the generation of age offsets, have potential to be coupled: bioturbational mixing of sediment and bioirrigation enhance aerobic degradation of organic matter and shift the redox boundary downward (Kristensen, 2000), affecting the preservation of carbonate shells that respond to changes in pore-water chemistry (Aller, 1994). Activities of burrowers can thus represent a key driver of the disintegration of shells in sediments, creating a *taphonomic active zone* (TAZ, Davies et al., 1989) of elevated shell destruction by microbial and other destructive processes (e.g., scavenging, bioerosion, and abrasion). Here, we define the TAZ purely on the basis of physical, biological, and geochemical activities that affect the preservation state of the shell. Although some of these activities can enhance durability (e.g., encrustation and diagenetic replacements), they primarily contribute to shell disintegration. The TAZ contrasts with the sequestration zone (SZ, Tomašových et al., 2014), where disintegration and other taphonomic activities become negligible. Movement of a shell is

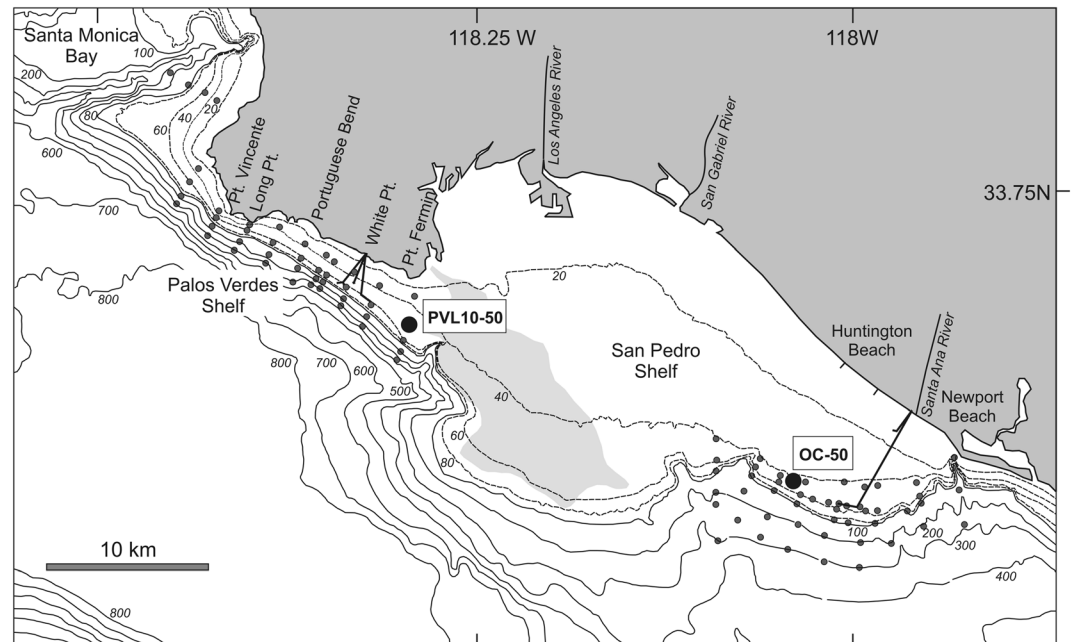


**Figure 2.** Geographic location of two coring sites (large circles) in 50-m water depth on the Palos Verdes Shelf (station PVL10-50) and the San Pedro Shelf (station OC-50) in Los Angeles and Orange Counties, California. Gray-shaded region represents seafloor with exposed Miocene and Pliocene sedimentary rocks (Fisher et al., 2004; Nardin & Henyey, 1978); small dots are stations with regular sediment monitoring by Los Angeles County and Orange County, associated with their ocean wastewater outfalls (black lines). Map adapted from Stull et al. (1996) and Maurer et al. (1993).

thus not in itself a taphonomic activity, although it may increase (or decrease) preservation by shifting a shell into a layer with higher (or lower) taphonomic activity.

Although it can be assumed that the TAZ overlaps completely and exclusively with sediment layers affected by bioturbational mixing and bioirrigation (e.g., Cherns & Wright, 2011), it is unclear whether the boundary between the TAZ and the SZ is located within the SML, coincides with the base of the SML, or extends some depth down into the IML. Here, we explicitly distinguish between the depth of the TAZ and these mixing layers and show that the key factor determining the creation of age offsets is the relationship between the base of the TAZ (determining where disintegration rates become negligible) and the depth of maximum bioturbation (determining the potential for exhuming older age cohorts back toward the surface by bioadvection).

We assess the interplay between sedimentation, mixing, shell disintegration, and shell production using new data on downcore changes in the AFDs of two bivalve species in cores from the open continental shelf of Southern California (Figure 2), based on 849 shells dated by radiocarbon-calibrated amino acid racemization (AAR), and evaluate both within-species and between-species age offsets. We show that (1) age offsets cannot be predicted simply from estimates of sedimentation rate and the thickness of the surface mixed layer (SML); (2) the IML is located below the TAZ, and thus, old shells from the SZ can be exhumed back into the SML and thus admixed with young shells that are degrading at a high rate; and (3) between-species differences in the history of shell production magnify between-species age offsets within any of these sedimentary increments.

## 2. Material and Methods

### 2.1. Setting

The Palos Verdes and the San Pedro shelves of Southern California (Figure 2) present a depositional mosaic dominated by muddy and sandy sediments, with shelf-edge regions formed by condensed and relict sediments (Emery, 1952); spatially variable sedimentation rates, with a general offshore decrease (Alexander & Lee, 2009); and diverse burrowing organisms that penetrate to 20- to 30-cm sediment depth (Swift et al.,

1996). Both shelves have wastewater outfalls at ~60-m water depth (Diener et al., 1995; Stull et al., 1996). During the twentieth century, sedimentation rates were enhanced locally by deposition of wastewater effluent (Lee et al., 2002; Niedoroda et al., 1996).  $^{210}\text{Pb}$  profiles imply that, during times of maximum discharge in the 1960 to 1970s, net sedimentation rates were 1–2 cm/year at sites proximal to these outfalls and 0.6–1.2 cm/year at distal sites still within the effluent zone (Santschi et al., 2001); pre-effluent sediment accumulation rates based on  $^{210}\text{Pb}$  profiles were 0.17–0.35 cm/year (Alexander & Lee, 2009). Longer-term rates of sedimentation based on downcore foraminifera shell ages indicate order-of-magnitude slower rates (~0.01–0.025 cm/year at site 3C and 0.06–0.1 cm/year at site 6C on the western Palos Verdes shelf; Santschi et al., 2001), in line with the observation of Sadler (1981) that net sedimentation rate decreases with the time span of measurement (Schumer et al., 2011; Paola et al., 2018). The overall thickness of postglacial Holocene sediments on these shelves is spatially variable, ranging between 1 and 25 m (McNeilan et al., 1996; Nardin, 1983; Sommerfield et al., 2009).

On the Palos Verdes shelf, small outfall pipes (1.5 m in diameter) terminating at 34-m water depth operated between 1937 and 1958, larger pipes terminating at 34 and 49 m operated between 1947 and 1966, and two Y-shaped outfalls (2.3 m in diameter) terminating at 60-m water depth have operated since 1956 and 1966 (Stull et al., 1996). Orange County opened an ocean outfall terminating at 18-m depth in 1927, and a larger outfall at 60-m water depth has operated since 1971 (Maurer et al., 1999; Smith, 1974). Bottom currents generally flow northward and westward along the Palos Verdes and San Pedro shelves, deflecting the wastewater emissions northwestward along the coast. Benthic communities were first sampled quantitatively during 1952–1956 (Hartmann, 1966) and 1956–1959 (Allan Hancock Foundation, 1965; Jones, 1969) and have been monitored regularly since 1972 on the Palos Verdes shelf (Ferraro et al., 1991; Stull et al., 1996) and since 1970 on the San Pedro shelf (Diener et al., 1995). To reconstruct changes in the living abundance of our key taxa *Nuculana taphria* and *Parvilucina tenuisculpta* in the late twentieth century, we used standardized community data produced since 1972 by the Los Angeles County Sanitation Districts (LACSD) and since 1985 by the Orange County Sanitation District (Maurer et al., 1993; Stein & Cadien, 2009; Stull, 1995) and combine them with earlier surveys performed in the 1950s by Hartmann (1966) and Allan Hancock Foundation (1965) and in 1970–1971 by Smith (1974).

## 2.2. Sampling

Boxcores and vibracores were acquired from 50-m water depth in September 2012 at one station on the Palos Verdes shelf (Los Angeles County, PVL10-50) and one station on the San Pedro shelf (Orange County, OC-50; Figure 2). PVL10-50 (33.6807°N, –118.3002°W) is located on the upcurrent margin of the wastewater plume from the White's Point outfall (Ferré et al., 2010), about 4 km SE of the southern outfall. Based on total nitrogen concentrations and mapping of the effluent layer thickness (Lee et al., 2002; Stull et al., 1986), this station is located outside of the effluent layer deposition. Coring station OC-50 (33.5885°N, –118.0416°W) is located about 4 km downcurrent and NW of the western termination of the Orange County outfall and is also not affected by effluent deposition (Anderson et al., 1993). At both stations, several 50-cm-long boxcores with 50-cm × 50-cm area were subsampled using as many as nine 15 × 15-cm clear plexiglas subcores, and several 100- to 150-cm-long vibracores of 8-cm diameter were also collected. At both stations, one boxcore and one vibracore was used for analyses of  $^{210}\text{Pb}$  activity and granulometry (BC1 and VC1 at PVL10-50 and BC1 and VC5 at OC50; VC5 misses the top 10 cm as indicated by onset of shell bed at 10–12 cm rather than at 20 cm as in boxcores). According to the reconstruction of relative sea level changes in the Southern California by Nardin et al. (1981), sites at 50-m depth were flooded ~13,000–14,000 years ago.

Dating and paleoecological analyses combine bivalve assemblages from both boxcores and vibracores at each site. At PVL10-50, abundances of bivalve species were counted in seven subcores collected from two boxcores (surface area equal to 0.1575 m<sup>2</sup>) and in three vibracores (VC3, 4, and 5, split to half-samples, with total surface area = 0.0075 m<sup>2</sup>). At OC-50, abundances of bivalve species were counted in three subcores collected from two boxcores (surface area equal to 0.0675 m<sup>2</sup>) and in two vibracores (VC6 and 7, 0.005 m<sup>2</sup>). The boxcores were extruded into 2-cm-thick increments in the upper 20 cm, and vibracore samples were cut into 4-cm-thick increments. To account for natural changes in shell content or grain size during incremental sampling, some analytical increments were thicker (3 or 5 cm thick).

To compare abundances between boxcores, vibracores, and LACSD-10C live-animal sampling sites, the 2-cm-thick core increments were pooled into 4-cm-thick increments, and abundance counts of mollusks

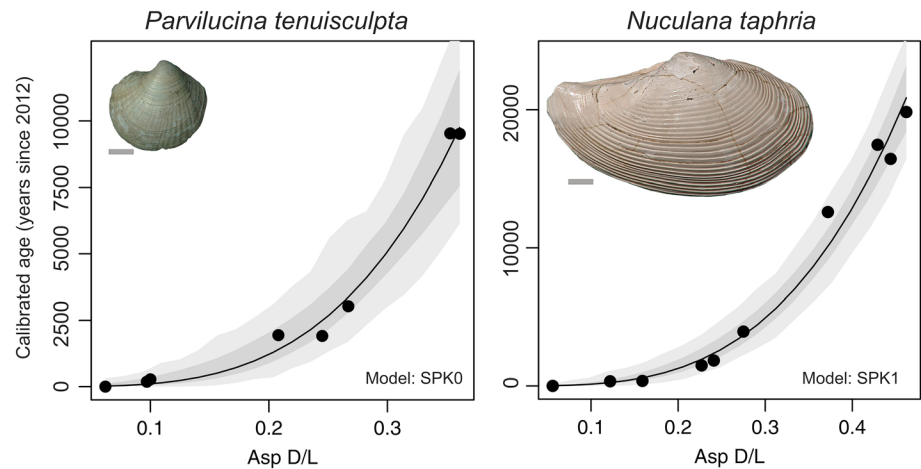


**Figure 3.** Relations between Asp D/L and  $^{14}\text{C}$  calibrated shell ages for *Parvilucina tenuisculpta* and *Nuculana taphria*, fitted with a simple power law kinetics model, assuming gamma (*P. tenuisculpta*) and lognormal (*N. taphria*) distributions for the residuals and including data from live-collected specimens as calibration data points. Light gray envelopes correspond to 95% prediction intervals for the age of a given specimen; dark gray envelopes correspond to 95% confidence intervals for mean age. One-millimeter scale bar in photographs of two specimens (vibracore samples from OC50).

were scaled up to  $0.1575\text{ m}^2$ , a spatial resolution comparable to the Van Veen grabs used in benthic monitoring. Complete valves and fragments with umbo preserved were selected from the  $>1\text{-mm}$  sieve fraction of each increment, counted and identified to species level. For each species, the maximum number of either left or right valves was added to the number of double-valved specimens to get the final count of fossil individuals in each increment. At both PVL10-50 and OC-50, bivalve species were also counted in two 100- to 150-cm-long vibracores. Shells of the two infaunal bivalve species—deposit-feeding *N. taphria* and chemosymbiotic were selected for age dating, building on our previous work on these species using Van Veen samples (Tomašových et al., 2014). *P. tenuisculpta* prefers muddy sediments with organic enrichment and tolerates moderate pollution (Fabrikant, 1984), whereas *N. taphria* rather prefers sandy sediments and is sensitive to contamination (Zmarzly et al., 1994). Boxcore and vibracore increments were correlated based on changes in lithologic content, shell abundance,  $^{210}\text{Pb}$  profiles, and shell age data.

### 2.3. AAR and $^{14}\text{C}$

Core chronology is based (1) on the radiocarbon-calibrated AAR dating of two bivalve species, *N. taphria* and *P. tenuisculpta* (Figure 3) and (2) on the  $^{210}\text{Pb}$  activity profile of near-surface sediment. *N. taphria* is an infaunal deposit feeder (our dated shells are 3–15 mm in length at both sites) living close to the sediment surface. *P. tenuisculpta* is an infaunal facultative chemosymbiont-bearing bivalve (2–10 mm in length at PVL10-50 and 2–5 mm in length at OC-50). Twenty randomly selected specimens (complete valves or fragments with umbo preserved) or less (if the number of available specimens was smaller) of *N. taphria* and *P. tenuisculpta* were selected from 4-cm-thick increments from boxcores (BC1 at PVL10-50 and BC1-3 at OC-50). Similarly, 20 specimens (or less) of each species were selected from vibracore increments of PVL10-50-VC5 (upper 52 cm) and OC-50-VC6 (upper 85 cm). Additional three shells of *N. taphria* were dated from 195 to 200 cm at OC50-VC6.

A total of 159 and 111 specimens of *P. tenuisculpta* and a total of 255 and 336 specimens of *N. taphria* from PVL10-50 and OC-50 were selected for AAR analyses from the  $>1\text{-mm}$  sieve fraction. 266 dead specimens of *P. tenuisculpta* and 583 dead specimens of *N. taphria* passed the AAR screening criteria of Kosnik and Kaufman (2008; Table S1, all data are also deposited at doi.pangaea.de/10.1594/PANGAEA.900879).  $^{14}\text{C}$  data to calibrate AAR were presented in Tomašových et al. (2014). To improve the calibration of *P. tenuisculpta*, we measured two new specimens of *P. tenuisculpta* with high D/L values from 62 to 66 cm in PVL10-50-VC5 at the NOSAMS facility, Woods Hole.  $^{14}\text{C}$  of all specimens were recalibrated to calendar years using Calib6.0 (Stuiver & Reimer, 1993), the Marine13 data (Reimer et al., 2013), and a temporally variable regional marine reservoir correction (Hendy et al., 2013; Table S2).

The extent of AAR was analyzed with reverse phase high pressure liquid chromatography (Kaufman & Manley, 1998). The rate of AAR was calibrated using the Bayesian model fitting according to Allen et al. (2013). The calibration of AAR in *P. tenuisculpta* is based on seven dead specimens dated with  $^{14}\text{C}$  one live-collected specimen (where D/L values are averaged across two replicates, Table S2), using the simple power law kinetics model (SPK0, Allen et al., 2013) for Asp D/L, with the initial D/L value set to zero (Figure 3). The calibration equation for *P. tenuisculpta* is  $a\text{DL}^b$ , where DL is Asp D/L, and  $a = 354578.1$  and  $b = 3.527$ . The uncertainty is defined by the gamma distribution, with the shape parameter equal to 143.238. The calibration of AAR in *N. taphria* is based on nine specimens dated with  $^{14}\text{C}$  and one live-collected specimen (Table S2). It is based on the simple power law kinetics model (SPK1) for Asp D/L, with the initial D/L value estimated from data (Figure 3). The uncertainty is defined by the lognormal distribution, with the standard deviation parameter equal to 0.05691097. The calibration equation for *N. taphria* is  $a(\text{DL}^b - \text{DL}_0^b)$ , where  $a = 248346.4$ ,  $b = 3.282783$ , and  $\text{DL}_0 = 0.055$ . These Bayesian calibrations improve upon those published using nonlinear least squares regressions of postmortem ages of *N. taphria* and *P. tenuisculpta* derived from surface samples (Tomašových et al., 2014, Table S1). Below, we refer to ages in terms of calibration years before the time of core sampling, which was 2012 CE (rather than before 1950 CE to avoid negative ages of shells that died in the late twentieth century).

Sediment increments with dated shells were assigned to three stratigraphic units on the basis of changes in grain size and shelliness (Table S4). Shell age-frequency distributions overlap to some degree between these units. Therefore, in addition to median shell age, their geochronologic determination is based on the 25th and 75th shell age percentiles. Net burial rates of shells based on shell age data are based on differences in median ages between depth midpoints of stratigraphic units, with uncertainty based on 95% confidence intervals on per-unit shell median age.

#### 2.4. $^{210}\text{Pb}$ and $^{137}\text{Cs}$

Activities of  $^{210}\text{Pb}$ ,  $^{226}\text{Ra}$ , and  $^{137}\text{Cs}$  were quantified in 2-cm-thick intervals in the upper 40 cm from one box-core and one vibracore at each site (Table S3). All radionuclides were quantified using gamma spectroscopy as described in Alexander and Lee (2009). The SML as indicated by vertical profiles in excess  $^{210}\text{Pb}$  is  $\sim 10$  at PVL10-50 and  $\sim 15$  cm thick at OC-50. Apparent sedimentation and sediment accumulation rates were computed from the slope of the decay in excess  $^{210}\text{Pb}$  below this SML using the Constant Flux-Constant Sedimentation model (Sanchez-Cabeza & Ruiz-Fernandez, 2012). The slope terminates where the excess  $^{210}\text{Pb}$  activity falls to the  $^{226}\text{Ra}$  supported values, which was at 30- or 40-cm depth at both sites.  $^{137}\text{Cs}$  values are expected to peak at 1971 CE in sediments of the Palos Verdes shelf, delayed from the commonly observed 1963 CE peak by the intermittent nature of runoff from the semiarid watershed (Santschi et al., 2001).

#### 2.5. Within- and Between-Species Age Offsets

We assess within- and between-species age offsets both at the scale of 4-cm-thick sedimentary increments and at the scale of five  $\sim 20$ -cm-thick stratigraphic subunits created by pooling data from 4-cm increments. Within-species age offsets (i.e., within-species time averaging) were estimated for *N. taphria* and *P. tenuisculpta* using the interquartile range (IQR) of their shell ages corrected for the calibration error and computed as the difference between the raw IQR on one hand and the error component on the other hand (Dominguez et al., 2016; Ritter et al., 2017). The calibration error alone was estimated as the mean IQR of all shells in a given increment, where an IQR for each shell was computed on the basis of a repeated sampling of log-transformed ages from lognormal (*N. taphria*) and gamma distributions (*P. tenuisculpta*). The between-species age offset corresponds to the difference between the median ages of two species within the increments or within the subunits.

Under steady-state sedimentation, the residence time of sedimentary particles and thus their time to burial are exponentially distributed (Olszewski, 2004; Tomašových et al., 2014). Therefore, IQR is expected to equal a logarithm of three divided by an inverse of transit time below the completely-mixed SML (i.e., SML thickness divided by burial rate of shells). We assess whether this expectation can account for the empirical IQR. The median depths of 1,000-year age cohorts can estimate the original source depths of shells that were shifted upward or downward by bioturbation. When bioturbational mixing is complete, median shell depths can be expected to be located in the middle of this depth range. When mixing is incomplete, the asymmetry of the shell depth distributions under incomplete mixing should be diagnostic of cohort source depths, even though some shells from this cohort can be shifted significantly upward or downward by nonlocal feeders.

## 2.6. Loss Rates

AFDs can be used to infer the rate of shell loss from a surface sediment layer, either by disintegration or by burial (and burial may be either by net sediment accumulation or by downward bioadvection; Tomašových et al., 2014, 2016). AFDs from samples of surficial sediments (top 15 cm) acquired during past benthic surveys and from our core Unit 1 (20–24 cm) at both stations because (1) such surface increments do not lose shells by exhumation to overlying increments and (2) assumptions about production in recent time can be confirmed on the basis of monitoring data. To minimize the effects of temporally variable production on estimates of loss and to reduce the effects of site-to-site variation, we assess loss rates using AFDs by pooling AFDs from 14 sites with *P. tenuisculpta* ( $n$  dated specimens = 232) and 10 sites with *N. taphria* ( $n$  = 146), all acquired from Van Veen grabs collected in 2003 in the Southern California Bight (Tomašových et al., 2014); we excluded sites deeper than 60 m to avoid assemblages from the San Diego Shelf with relict shells older than 10,000 years not associated with active production (Tomašových et al., 2016).

Given that AFDs for both species are right-skewed and thus do not suffer from inactive production over the past decades and centuries, we estimate loss rates by fitting these shell AFDs from the upper seabed to one- and two-phase exponential models that assume constant production (Tomašových et al., 2014, 2016). The one-phase model assumes that disintegration rate does not change either with shell age and/or with its depth within the TAZ. In contrast, the two-phase model permits a decline in disintegration rate (from  $\lambda_1$  to  $\lambda_2$ ) with increasing shell age due to shell sequestration, which gives the shell a respite from loss and thus promotes long-term preservation. Sequestration (quantified by the rate parameter  $\tau$ ) might be achieved by temporary or permanent burial below the TAZ, where loss rates from disintegration are expected to be lower, and/or by diagenetic stabilization at any depth within the seabed (Tomašových et al., 2014).

Monitoring data show that populations of *Parvilucina* declined strongly during the late 1980s (Leonard-Pingel et al., 2019). Therefore, we also estimate the rate of shell loss for this species by adjusting the one-phase and two-phase models to account for the low abundance of this species over the past 20 and 25 years, relative to 2012 CE (parameter  $T_{\min}$  in Tomašových et al., 2016). In the age unmixing procedure (next section), we use loss rates based on the fit of the two-phase model to AFDs of spatially pooled surface assemblages from the entire Southern California Bight (Table S5).

## 2.7. Age Unmixing

Two steps are required to unmix assemblages of dated specimens (i.e., disarticulated valves) on the basis of their AFDs (Tomašových et al., 2017), that is, to recover pre-bioturbation temporal patterns in the abundance of two species by sorting them into age cohorts. First, for each 4-cm increment, information from the AFD of dated shells (a subset of all specimens present in that increment) was bootstrapped up to apply to all specimens of that species in that increment. The number of resampled specimens in 10-year cohorts was counted after this resampling procedure. The shape of the AFDs in the few increments that did not contain any directly dated specimens was interpolated on the basis of AFDs from the underlying and overlying increments. The abundance of specimens in each cohort estimated by this step does not account for specimens that were lost by disintegration (see second step) nor by burial to increments beyond core penetration, which was probably negligible. At PVL10-50, increments below the dated increments are laminated and thus burial of specimens to such depths was unlikely. At OC-50, bivalve abundance abruptly declines below 85 cm in vibracore VC6 and below 130 cm in vibracore VC7.

In the second step, we analytically restore specimens likely lost from disintegration, using the estimates of  $\lambda_1$ ,  $\lambda_2$ , and  $\tau$ . The predicted number of preserved specimens (at the resolution of 10-year cohorts) was divided by the survival function of the best-fit model (Tomašových et al., 2016), generating the original, “preloss” number of specimens (scaled to 0.15 m<sup>2</sup>). To compute the standing density of living individuals, this number is halved because the total number of specimens in increments is based on the sum of disarticulated valves (i.e., maximum number of individuals; no valves were articulated).

## 3. Results

### 3.1. Core Stratigraphy and Downcore Changes in Shell Ages

Both cores can be subdivided into three distinct units differentiated by grain size and fossil abundance. These units are relatively age-homogeneous based on dated shells; that is, the median ages of 4-cm-thick

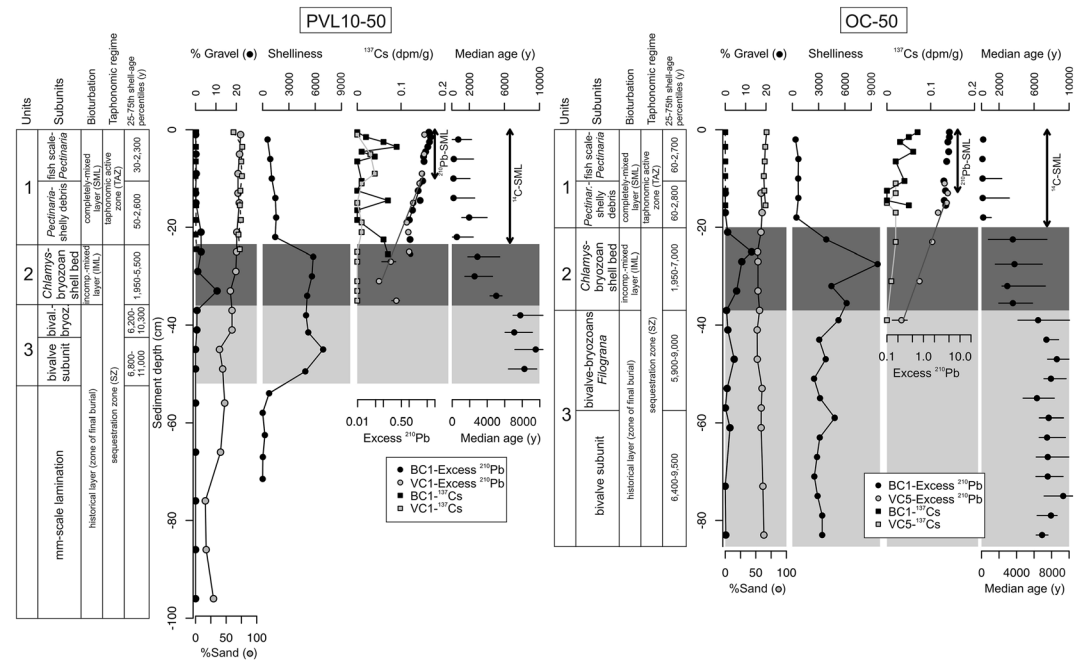


**Figure 4.** Stratigraphic subdivision of sediment cores into three main units based on generalized lithology (top Unit 1 of bioturbated silty sand/sandy silt, Unit 2 of a sandy *Chlamys*-bryozoan muddy shell bed, and Unit 3 of bivalve-rich sandy silt; at PVL10-50, underlain by laminated silt), five subunits discriminated using fossil content, and zones differing in bioturbational mixing and in taphonomic regime, along with downcore changes in grain size, shelliness (total abundance of shells >1 mm per 4-cm increment), excess <sup>210</sup>Pb (dpm/g), <sup>137</sup>Cs (dpm/g), and amino acid racemization (AAR) median shell ages (with 25th and 75th age quantiles) as calibrated by <sup>14</sup>C. Double-headed arrows at the top refer to the thickness of the surface completely-mixed layer (SML) as indicated by age-homogeneous profiles in <sup>210</sup>Pb and in <sup>14</sup>C-AAR shell ages. Our definition of the surface completely-mixed layer (SML) refers to age homogeneity of <sup>14</sup>C-AAR shell ages. Median ages of 4-cm increments (black dots in far right columns; lines are interquartile ranges) are calculated using all shell ages of *Nuculana taphria* and *Parvilucina tenuisculpta* at both stations.

increments do not markedly increase downcore within each unit (Figure 4). Although the 25th and 75th age percentiles of stratigraphically-adjacent units overlap to some degree (Figures 4 and 5), median ages increase downcore overall from Unit 1 to Unit 2 and from Unit 2 to Unit 3. The lower half of the core at PVL10-50 is formed by a laminated shell-poor silt that yields no shells of *N. taphria* and *P. tenuisculpta* and thus is not considered further. Units 1 (20–24 cm thick) and 2 (16–17 cm thick) have similar thicknesses at the two sites, but Unit 3 attains 15 cm at PVL10-50 and ~55 cm at OC-50. Sands with dispersed bivalves (the razor clam *Ensis*) and fragments of sand dollars occur between 90- and 200-cm core depths, and shell-poor silty sediments rich in charcoal and plant remains appear at 200 cm at OC-50.

Unit 1 comprises relatively shell-poor muddy sands with median shell ages <700 years (Figure 4). It extends 0–24 cm at PVL10-50 (entirety of those boxcores) and 0–20 cm at OC-50 (entire box core and upper part of vibracore), with the 25th and 75th shell age percentiles ranging between 30 and 2,600 years at PVL10-50 and between 60 and 2,800 years at OC-50. It can be subdivided into two subunits on the basis of faunal composition: an upper shell-poor subunit characterized by abundant fish scales and agglutinated-sand worm tubes (*Pectinaria*; Figures 4, 5a, and 5d) and a lower subunit characterized by *Pectinaria* and a higher abundance of molluscan debris (at 8–24 cm at PVL10-50 and at 12–20 cm at OC-50, Figure 5b). These two subunits are separated by abundant debris of the semiinfaunal bivalve *Modiolus* in the PVL10-50 core. Unit 2 is represented by a shell bed formed by muddy sands with abundant, densely- to loosely-packed *Chlamys* scallops, infaunal bivalves, and erect bryozoans (constitute the gravel fraction, Figure 4) between 24 and 36 cm at PVL10-50 (Figure 5c) and between 20 and 37 cm at OC-50 (Figure 5e), with median shell ages ranging between 3,300 and 3,600 years (25th and 75th shell age percentiles = 1,950–5,500 years at PVL10-50 and 1,950–7,000 years at OC-50). Unit 3 comprises shell-rich, sandy muds between 36 and 51 cm at PVL10-50 and at 37–100 cm at OC50, with median age 7,300–8,800 years at PVL10-50 (25th and 75th shell age percentiles = 6,200–11,000 years) and 7,500–7,700 years at OC-50 (25th and 75th shell age percentiles = 5,900–9,500

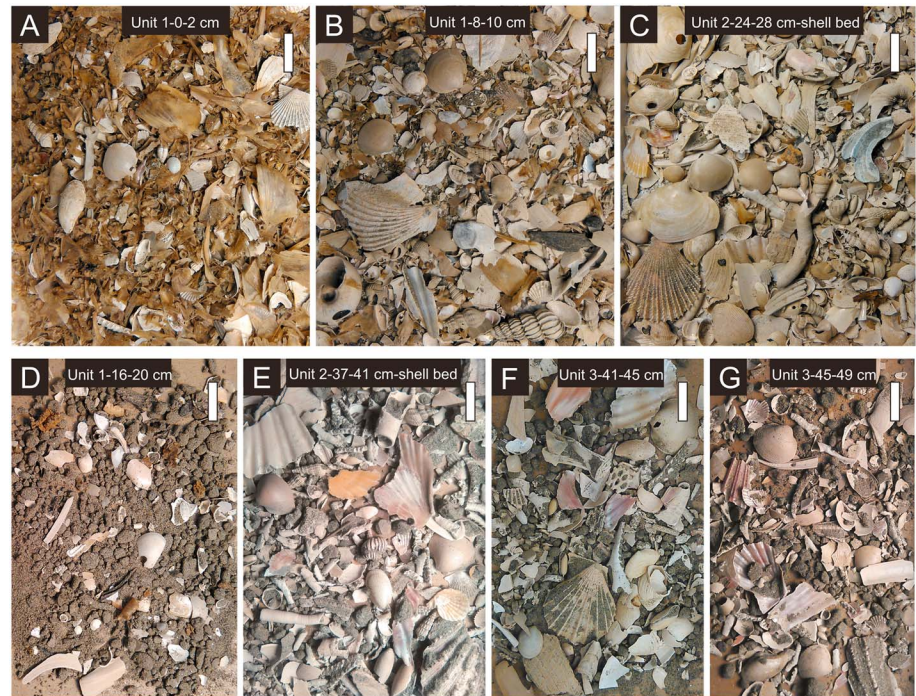


**Figure 5.** Examples of residues of death assemblages (sieved with 1-mm mesh size) at PVL-50 (boxcore residues) and OC-50 (vibracore residues) show the shift from shell-poor assemblages with fish scales and *Pectinaria* in Unit 1 (a, d) to the shell bed in Unit 2 (b, e) and bryozoan-bivalve-rich assemblages in Unit 3 (f, g). Vertical scale bar: 1 cm.

years). Scallops are less frequent than in Unit 2, but bryozoan debris is abundant in the upper part of Unit 3 at both sites (bivalve-bryozoan subunit; Figures 4, 5f, and 5g), and infaunal bivalves are abundant throughout. At OC-50, where Unit 3 is very thick, the upper subunit (37–57 cm) has shell-rich increments, including calcified serpulid worm tubes of *Filograna* and abundant balanid barnacle debris at ~50 cm.

### 3.2. Sedimentation Rates and Thickness of the SML

Within each unit, the AFDs of the 4-cm-thick increments and of the 10- to 20-cm-thick subunits tend to be similar in their median age and IQR (Figures 4–6). Based on differences in median shell ages between stratigraphic units, net burial rates of shells are very slow: 0.005–0.008 cm/year between Units 1 and 2 and 0.002–0.003 cm/year between Units 2 and 3 at PVL10-50, and 0.004–0.007 cm/year between Units 1 and 2 and 0.006–0.01 cm/year between Units 2 and 3 at OC-50. Shells at the base of OC-50-VC 6 at 200 cm are 9,000–10,400 years old, indicating that the late-transgressive sediments underlying Unit 3 were deposited at a higher rate (~0.05 cm/year). These  $^{14}\text{C}$ -based rates contrast with the apparent  $^{210}\text{Pb}$ -based sedimentation rate for the last ~100 years, which is ~0.2 cm/year at both stations. Sediment accumulation rates are 0.19–0.41  $\text{g}\cdot\text{cm}^{-2}\cdot\text{year}^{-1}$  at OC-50 and 0.25  $\text{g}\cdot\text{cm}^{-2}\cdot\text{year}^{-1}$  at PVL10-50. Small peaks in  $^{137}\text{Cs}$  peak occur at 3–4 and 14–15 cm in a boxcore and at 9 cm in a vibracore at PVL10-50, consistent with the  $^{210}\text{Pb}$ -based estimate.

Shell ages and  $^{210}\text{Pb}$  also give different perspectives on the thickness of the SML. The median shell ages of both species remain relatively constant downcore through the two subunits within Unit 1 at both sites (Figures 5a and 5c), suggesting that Unit 1 (20–24 cm thick) is almost completely mixed throughout the entire thickness. In contrast, values of  $^{210}\text{Pb}$  are homogeneous only in the upper 10 cm at PVL10-50, corresponding to the upper subunit of Unit 1, with declining excess  $^{210}\text{Pb}$  values in the lower, more shell-rich part (Figure 4). At OC-50, differentiation of Unit 1 into two subunits is less distinct physically, but  $^{210}\text{Pb}$  values are relatively homogeneous only in the upper 15 cm. Thus, the thickness of the SML is thinner on the basis of uniform  $^{210}\text{Pb}$  values (10–15 cm) than it is on the basis of age-homogeneous shell profiles (20–24 cm). Here, we define the SML on the basis of  $^{14}\text{C}$ -calibrated shell ages.

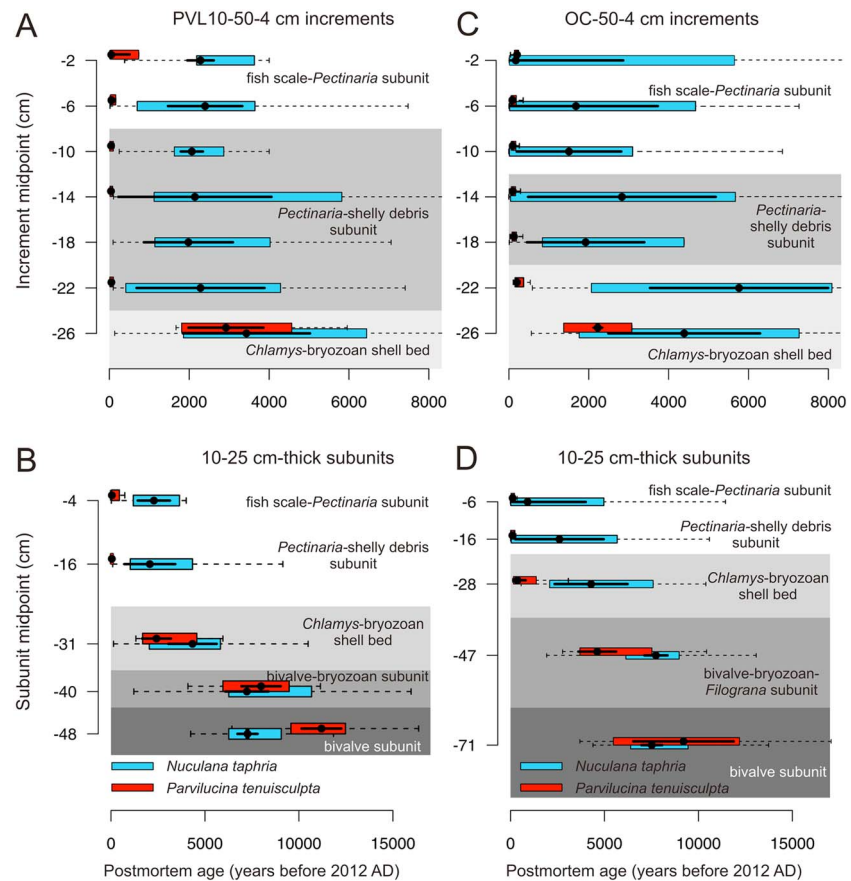


**Figure 6.** Top row: Within-species and between-species age offsets between *Nuculana* and *Parvilucina* in 4-cm-thick increments remain constant within the uppermost 20–25 cm (Unit 1) of cores; that is, there is no stratigraphic differentiation of age-frequency distributions within the upper 20–25 cm and *Parvilucina* is invariably younger than *Nuculana* (a, c). Boxplots are shaded by species. Bottom row: Pooling 4-cm increments into five 10- to 20-cm-thick subunits, the between-species age offsets become minor in the *Chlamys*-bryozoan shell bed (Unit 2), and are reversed in the two bivalve-rich subunits of Unit 3, where *Parvilucina* is older (b, d). Interquartile ranges of shell ages corrected for calibration error are shown as thick horizontal lines and are smaller than the differences between the 25th and 75th age percentiles based on calibrated shell ages.

### 3.3. Between-Species and Within-Species Age Offsets

The median ages of the two species within 4-cm increments of Unit 1 at PVL10-50 are separated by 1,000–2,000 years, with shells of *Parvilucina* being younger than shells of *Nuculana* (Figure 6a). Median ages become older and between-species age offsets become smaller in Unit 2 and PVL10-50 (Figure 6b). Trends are similar at OC-50: Median ages of *Parvilucina* and *Nuculana* are relatively homogeneous in the top 20 cm (Unit 1), with between-species age offsets >2,000 years (Figure 6c); the age difference persists into the *Chlamys*-bryozoan bed (Unit 2). The offset is reversed in Unit 3 at both sites, with shells of *Parvilucina* being older than shells of *Nuculana*, especially at PVL10-50 (Figure 6d). The downcore distribution of the median ages of bivalve shells thus indicates that the thickness of the completely-mixed layer on >100-year timescales at both sites is 20–25 cm rather than the 10–15 cm indicated by  $^{210}\text{Pb}$  activity (Figure 4).

Downcore, the right-skewed AFDs that characterize both subunits of Unit 1 (Figures 7a and 7b) are replaced by normal-shaped AFDs with shallower slopes in Units 2 and 3 (Figures 7c–7e). Time averaging (within-species age offsets, IQR) of *N. taphria* declines downcore from ~2,600 years in Units 1 and 2 to ~1,500 years in Unit 3 (Figure 6); this species is rare in living assemblages at midshelf depths over at least the last half century as documented in annual monitoring surveys in the Southern California Bight since the 1970s (Ferraro et al., 1991; Maurer et al., 1993; Stull, 1995). At OC-50, the IQR of *N. taphria* attains maximum values of 5,000 years in Unit 1 and declines downcore to 3,600 and ~1,100 years in Units 2 and 3 (Figure 6). In contrast, the

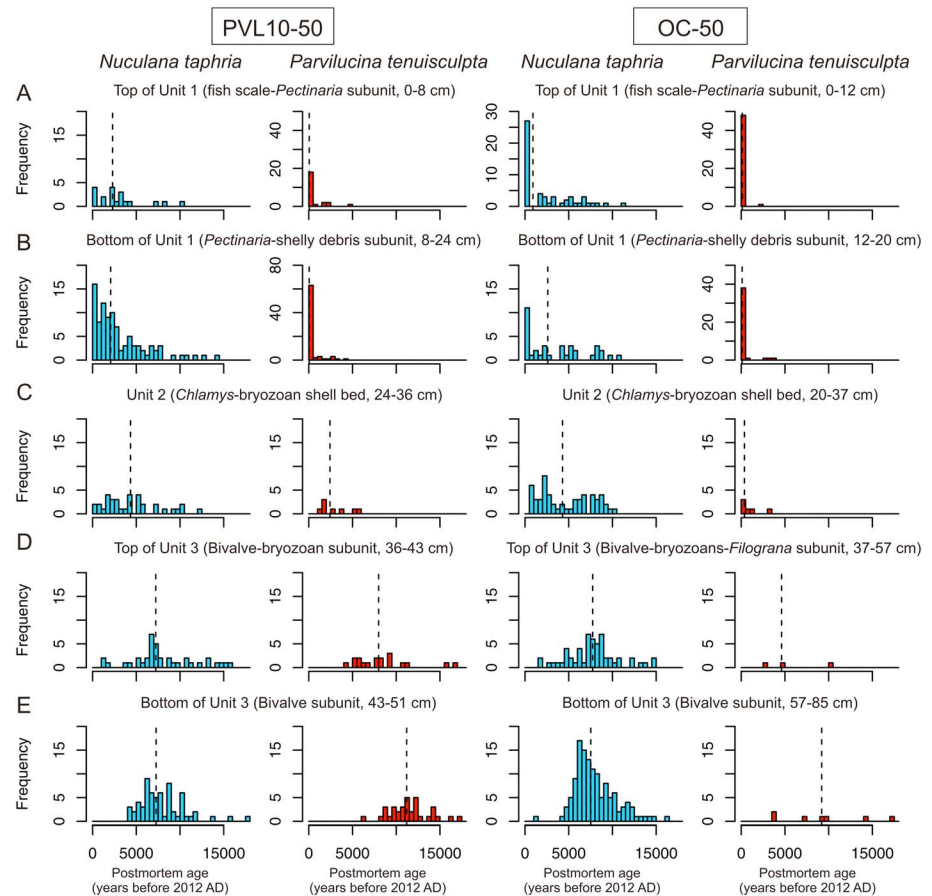


**Figure 7.** Downcore changes in the shape of the age-frequency distributions of *N. taphria* ( $n = 590$  shells) and *P. tenuisculpta* ( $n = 266$  shells) in five stratigraphic subunits (A-E) in cores from the Palos Verdes and San Pedro shelves, with a shift from strongly right-skewed, L-shaped distributions in the two top subunits (top 20–24 cm, Unit 1 in the two upper panels) to more symmetric, multimodal or unimodal distributions in deeper subunits (maximum core depth 51–91 cm, units 2 and 3 in the three lower panels). The vertical dashed lines denotes shell median age.

IQR of *P. tenuisculpta* is consistently low within Unit 1 at both sites (20 years at PVL10-50 and 10 years at OC-50); this species exhibited a strong, late twentieth century bloom on both shelves in response to wastewater input (Stull et al., 1996). The IQR of *P. tenuisculpta* increases to 3,000 years in Unit 3 at PVL10-50 and to 5,400 years at OC-50.

### 3.4. Loss Rates Based on Age Distributions From Unit 1 (SML)

Excepting *N. taphria* at PVL10-50, the AFDs of both species in Unit 1 are characterized by L-shaped, strongly right-skewed distributions: the highest frequency of shells is from cohorts <100 years old, and shells from cohorts >1,000 years old are less frequent but persistently present (Figures 8a–8f). Within the past 100 years, the frequencies of 10-year cohorts in the cores differ between *N. taphria* and *P. tenuisculpta*: For *N. taphria*, the two youngest cohorts (1990s and 2000s) are most frequent except at PVL10-50; for *P. tenuisculpta* the 1980 cohort of shells is the most frequent at both sites and in Van Veen grabs (upper 10–15 cm) from across the Southern California Bight (Figures 8g–8i).

AFDs of *N. taphria* show modes of 113 and 13 years, medians of 2,300 and 2,100 years, and IQRs of 3,000 and 5,600 years (Figures 8a and 8b). AFDs of *P. tenuisculpta* show very young modes of 24 and 80 years, medians of 44 and 106 years, and narrow IQRs of 65 and 144 years (Figures 8d and 8e). The AFDs of both species collected by Van Veen grabs are also L-shaped (Figures 8c and 8f), with similar contrasts between *N. taphria* (mode = 8 years, median = 60 years, IQR = 3,500 years) and *P. tenuisculpta* (mode = 40 years, median = 33 years, IQR = 55 years).

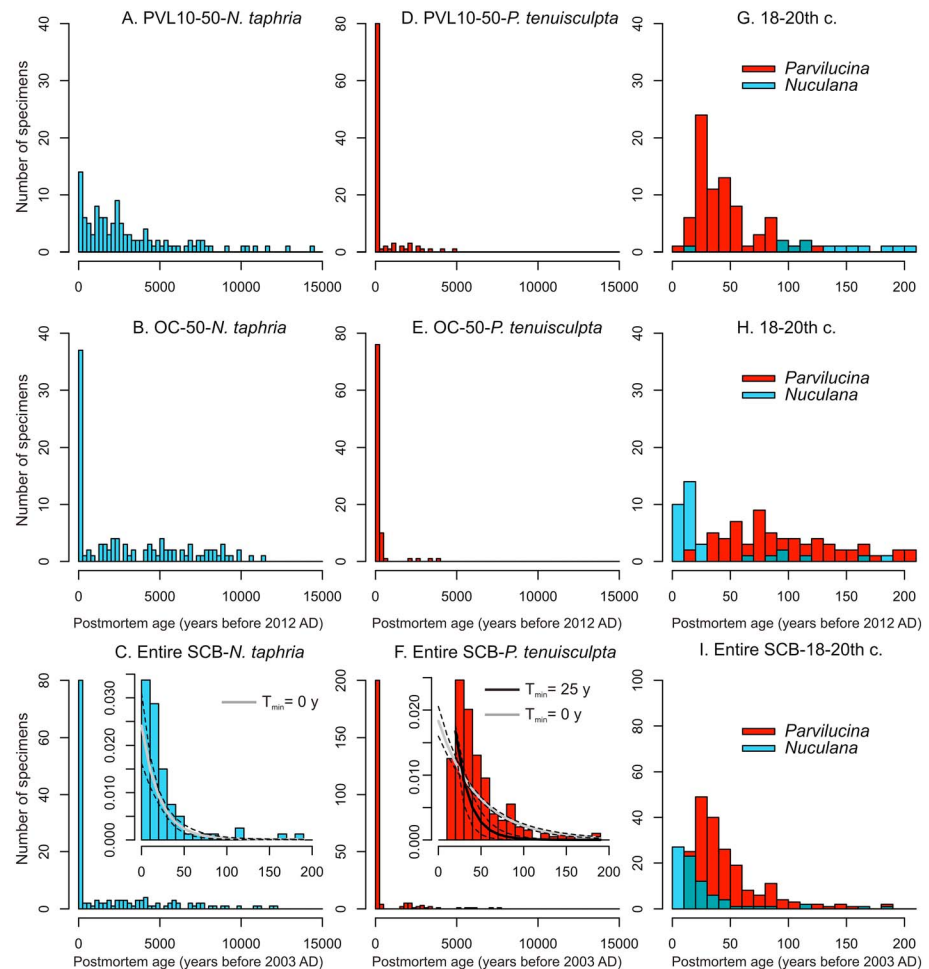


**Figure 8.** (a–f) The age-frequency distributions of shells of two bivalve species taken from the upper 25 cm (Unit 1) of cores at two sites (top and middle row, PVL10-50 and OC-50) and from Van Veen grab samples (top 10–15 cm) of shelves throughout the Southern California Bight (bottom row, SCB) are all strongly right-skewed and L-shaped, with many very young shells and a long tail of shells >1,000 years. The insets in the bottom row show the fits of the two-phase exponential model. (g–i) Overlapping age-frequency distributions of shells from only the last 200 years reveal (1) a peak in abundance of *P. tenuisculpta* shells ~30 years ago both at PVL10-50 and across the whole Bight (1970s to 1980s), corresponding to high emissions of wastewater, with the peak a bit earlier in the twentieth century at OC50, and (2) lower numbers of this species everywhere in the last few decades. In contrast, *N. taphria* has been very rare at PVL10-50 and elsewhere on the Palos Verdes shelf for most of the last two centuries, but has been steadily present and even rebounded at OC-50 and elsewhere in the Bight within the past 20 years. Postmortem ages are given in years relative to time of sampling (2012 CE for shells at PVL10-50 and OC-50; 2003 CE for shells from across the SCB).

Model fitting shows strong support for an age-dependent (i.e., a two-phase) model of decline in rates of shell disintegration for both species at both coring sites (excepting *N. taphria* at PVL10-50 where very young shells are rare) and for both species in Bight-wide van Veen assemblages (Table S5). The Bight-wide assemblages indicate an initial, short-term loss rate  $\lambda_1 = 0.021$  for *P. tenuisculpta* ( $\lambda_1 = 0.043$  at  $T_{\min} = 20$  years, and  $\lambda_1 = 0.06$  at  $T_{\min} = 25$  years) and  $\lambda_1 = 0.048$  for *N. taphria*, corresponding to decadal-scale half-lives in Unit 1. The sequestration rate  $\tau$  ranges between 0.0002 and 0.0005 in *P. tenuisculpta* and 0.0002–0.0005 in *N. taphria* (Figure S1)—that is, sequestration takes places at millennial timescales. The long-term loss rate  $\lambda_2$  is 2 orders of magnitude smaller than the short-term loss rate  $\lambda_1$  in both species (0.0003–0.0005 in *Parvilucina* and 0.0002–0.0003 in *Nuculana*; Figure S1). The similarity in time to final loss from Unit 1 (i.e., an inverse of  $\lambda_2$ ) to the timescale of net burial of shells based on downcore changes in median shell age (i.e., time to burial of a shell below the ~20-cm-thick Unit 1 is ~2,500–4,000 years under 0.005–0.008 cm/year at PVL10-50 and is ~2,900–5,000 years under 0.004–0.007 cm/year at OC-50) shows that the long-term loss rate  $\lambda_2$  corresponds to the rate of shell removal by burial.

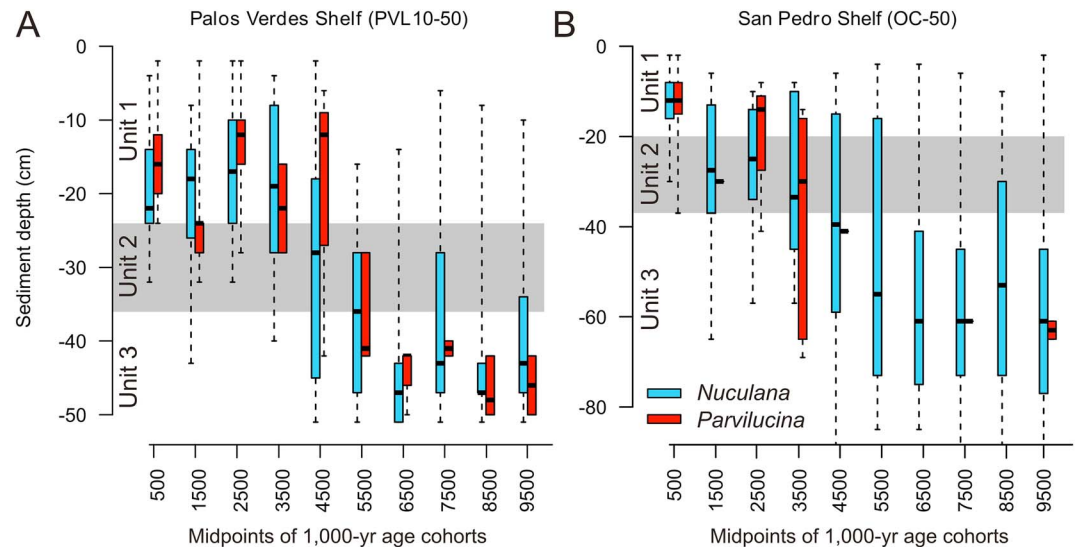


**Figure 9.** Stratigraphic distribution of 1000-year age cohorts, plotted using their age midpoints, shows that the shells of bivalves that lived within the past 2,000–3,000 years are mainly limited to the top 24 cm at PVL10-50 (Unit 1) (left panel) and largely occur at the boundary of Unit 1 (SML) with the Unit 2 shell bed at OC-50 (right panel). In contrast, shells from the 3,000–5,000 year cohorts, residing mostly in Unit 1, contribute to fossil assemblages in both the underlying and overlying units. *Parvilucina* at in the 4,500 and 7,500 cohort at OC-50 is represented just by a single specimen.

### 3.5. Sediment-Depth Distribution of Age Cohorts

Each 1,000-year age cohort is distributed over more than 20–30 cm at PVL10-50 and frequently over more than 40–50 cm at OC-50 (Figure 9), an interval that exceeds the thickness of the SML whether measured by shell ages (Unit 1; 20–24 cm) or by excess  $^{210}\text{Pb}$  (upper subunit of Unit 1, 10–15 cm; Figure 4). Incomplete mixing capable of exhuming old shells from depth up into a SML thus clearly operates at both sites. At PVL10-50, cohorts less than 4,000 years old are most abundant in Unit 1, extend partly down into Unit 2, and rarely contribute to Unit 3; cohorts spanning 4,000–6,000 years are centered on Unit 2 but extend into both the overlying and underlying units (Figure 9a). At OC-50, only the youngest cohort (<1,000 years) is limited almost entirely to Unit 1: Cohorts spanning 1,000–6,000 years tend to be centered on the Unit 2 shell bed and extend into both the overlying and underlying units. Cohorts >6,000 years old at both sites are centered in Unit 3, although they still contribute some shells to Unit 1 and Unit 2 (Figure 9b). The *Chlamys*-bryozoan shell bed at 20–40 cm at both sites (Unit 2) clearly represents a source for the *N. taphria* shells in Unit 1 that are older than ~4,000 years, demonstrating that the tail of older shells in Unit 1 AFDs reflects the exhumption of shells from deeper units (rather than shallow exhumption from basal increments of Unit 1).

### 3.6. Trends in Species Abundance Within Cores and After Age Unmixing

The proportional abundance of *P. tenuisculpta* attains a peak at the base of the Unit 3, is very low in Unit 2, and is highest in Unit 1 (Figure 10). At PVL10-50, its peak of 21% of the bivalve assemblage occurs at 10–12 cm, contrasting with only 0–5% in deeper increments, and occurs just below an increment rich in *Modiolus* debris that probably records a colonization event in 1985 (D. Cadien, LACSD, personal communication, 2018). At OC-50, the peak in proportional abundance of *P. tenuisculpta* (22%) occurs in the upper rather than in the middle parts of Unit 1 (Figure 10). Absolute abundances of *P. tenuisculpta* tend to be higher in Units 2 and 3 than in Unit 1 at PVL10-50 and remain rather uniform through the whole core at OC-50. In contrast, proportional abundances of *N. taphria* decline mildly upcore at PVL10-50 from 25% in Units 2–3 to 20% in Unit 1, and decline upcore more strongly at OC-50 from 40% to 10%. The decline of *N. taphria* from Unit 2 (shell bed) to Unit 1 is sharper in terms of absolute abundances at both sites (Figure 10).

The unmixed abundance trajectories of *P. tenuisculpta* show a moderate peak 10,000–12,000 years ago and a major increase in the twentieth century, exceeding former levels occurring during the Holocene by 2 orders of magnitude (Figures 10, 11a, and 11b). Such a major increase in the abundance of *P. tenuisculpta* in the late twentieth century at both sites is validated by monitoring surveys (Figure 11c). In contrast, the unmixed

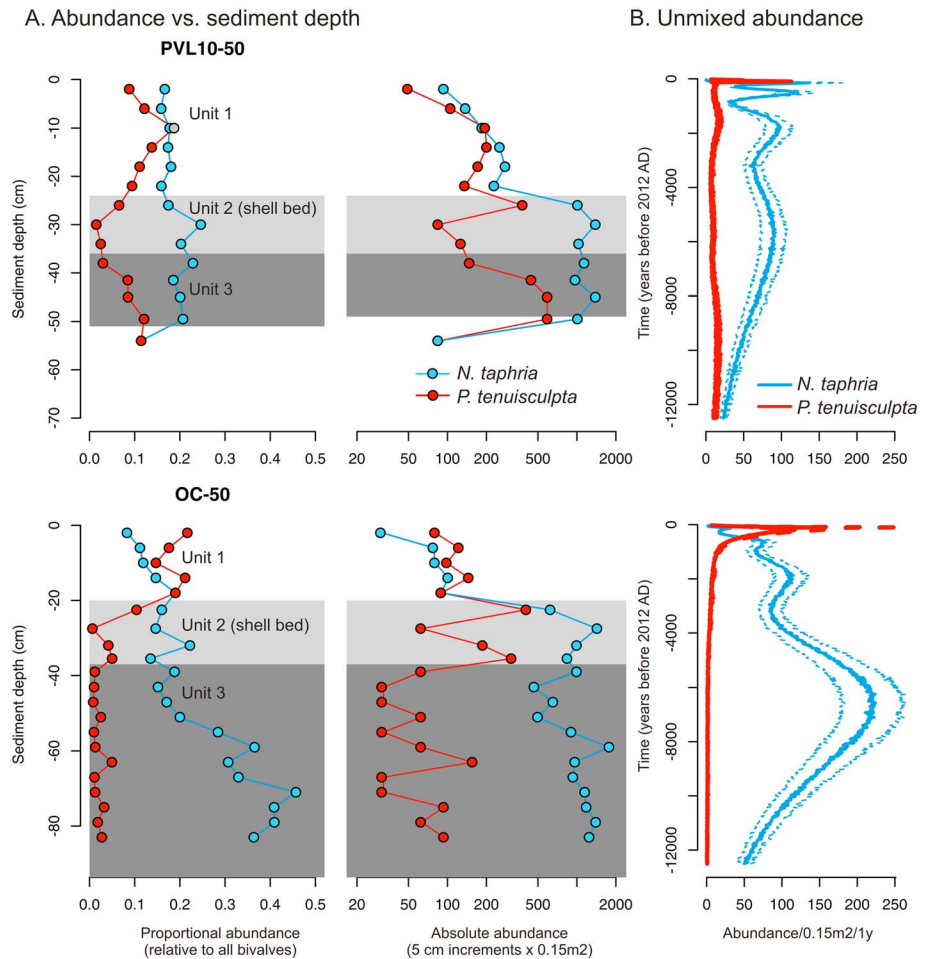


**Figure 10.** Changes in proportional (left panels) and absolute abundance (middle panels) of *Nuculana taphria* (blue) and *Parvilucina tenuisculpta* (red) in sediment cores scaled to depth (A), and their reconstructed trajectories in living abundance (individuals per 0.15 m<sup>2</sup> per 1 year, right panels) based on age unmixing (B) over the past 12,000 years on the Palos Verdes (top row) and San Pedro (bottom row) shelves. Age unmixing (B) detects a recentmost (last century) outbreak in *P. tenuisculpta* but also an earlier smaller peak in abundance ~10,000 years ago. It also detects a prolonged (multimillennial) increase (starting ~8,000 years ago) and an abrupt recentmost decline in abundance of *N. taphria* on both shelves. Raw stratigraphic patterns (A) do not detect either of these temporal changes, which have been blurred by bioadvective mixing.

abundance trajectories of *N. taphria* show a peak 5,000–7,000 years ago when water depth was ~10–20 m less than now at both sites. Its abundance remained high during the highstand phase, and declined significantly in the nineteenth century at PVL10-50 and probably earlier at OC-50, where its numbers were apparently always smaller (Figures 11a and 11b). Monitoring surveys indicate that *N. taphria* was rare on both shelves in the late twentieth century (Figure 11d). Comparison of stratigraphic trends in proportional abundances (Figures 10a and 10b) with unmixed abundances (Figure 10c) shows that (1) the recentmost increase in abundance of *P. tenuisculpta* has been smeared into the entirety of Unit 1, making the recentmost increase appear less dramatic (Leonard-Pingel et al., 2019), and (2) the recentmost decline in *N. taphria* is not detected in raw stratigraphic trends at PVL10-50. With the exception of these two discrepancies in the uppermost part of the cores, overall trends in unmixed abundances are qualitatively comparable to stratigraphic trends in proportional abundances.

## 4. Discussion

### 4.1. Mismatch Between <sup>210</sup>Pb and Shell-Based Estimates of Sedimentation and Mixing

The presence of a *Chlamys*-bryozoan bed of the same age (~3,000–6,000 years) at both sites only ~20 cm below the sediment-water interface indicates that long-term sedimentation rates at both sites are slower

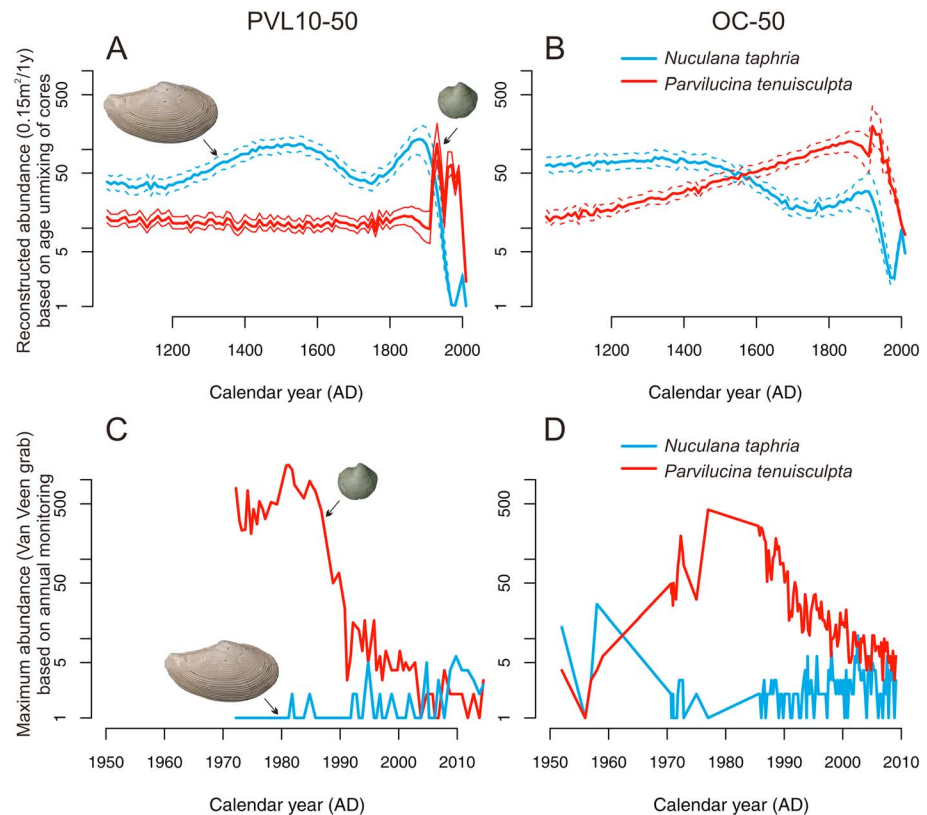


**Figure 11.** Comparison of reconstructed variation in abundance over the last 1,000 years with variation in abundance of living populations observed in the late twentieth century. (a and b) Reconstructed trajectories in living abundance of *P. tenuisculpta* and *N. taphria* (individuals per 0.15 m<sup>2</sup> per 1 year) based on age unmixing. (c and d) Temporal variability in maximum standing abundance (i.e., maximum across all grab samples in a given year) of *P. tenuisculpta* and *N. taphria* on the Palos Verdes shelf (between 30 and 60 m at line 10 near PVL10-50 core site) and on the San Pedro shelf (entire shelf at depths between 30 and 100 m) based on annual monitoring by wastewater agencies.

than expected on the basis of <sup>210</sup>Pb profiles. Estimates of apparent sedimentation rate based on <sup>210</sup>Pb (~0.2 cm/year) are faster than *long-term* sedimentation rates based on <sup>14</sup>C-calibrated bivalve shell ages (~0.005 cm/year) by 2 orders of magnitude. Our <sup>210</sup>Pb-based sedimentation rates are consistent with other radionuclide profile-based estimates for fine-grained particles in the late twentieth century at nearby sites on the Palos Verdes and San Pedro shelves that were not affected by the deposition of effluents in the late twentieth century (0.23–0.27 cm/year; Alexander & Lee, 2009; Santschi et al., 2001). The mismatch between the <sup>210</sup>Pb-based and <sup>14</sup>C-based ages in Unit 1 and the smearing of the <sup>137</sup>Cs peak indicates that the <sup>210</sup>Pb-based estimates of sedimentation are partly biased upward by a simple diffusional bioturbation (cf. Henderson et al., 1999; Kuzyk et al., 2015). However, simple diffusion that affects the vertical distribution of shells and <sup>210</sup>Pb-carrying particles equally cannot fully explain this age mismatch, because <sup>210</sup>Pb profiles are not homogeneous within Unit 1, whereas median shell ages are homogeneous within the same unit. Therefore, the mismatch of rates reflects differences in timescale of mixing between (a) relatively durable shells (bivalve shells initially degrade quickly but their disintegration rate declines significantly with their age, from decadal to millennial half-lives; Tomašových et al., 2014) and (b) the shorter-lived <sup>210</sup>Pb carried by fine-grained particles (half-life of 22 years). Less durable particles (here <sup>210</sup>Pb adsorbed on sediment grains) integrate the mixing process over a shorter time than more durable particles (here shells) and are thus less likely to be affected by infrequent but deep bioturbation events (Thomson et al., 1995, 2000).

Such differences in durability also translate to age differences within a single increment, that is, an analog of the Barker Effect (age differences that are generated by differences in the durability of fragile and robust foraminifer species, or between fragments and complete tests, Barker et al., 2007; Broecker & Clark, 2011). A

similar difference between  $^{210}\text{Pb}$  and  $^{14}\text{C}$  ages was also reported at two stations NW of the White Point outfall at 60-m water depth (Santschi et al., 2001), where muddy deposits 0–120 cm below the sediment-water interface contain foraminifer shells ranging in age between 3,000 and 10,000 years. Although size-selective bioturbation processes can either preferentially mix smaller particles (e.g., Wheatcroft, 1992) or preferentially advect larger particles upward (e.g., McCave, 1988), such processes should not generate higher age homogeneity among larger shells, such as observed here.

Under slow sedimentation rates, when the time to permanent burial exceeds the time to disintegration, any difference in durability between age tracers will generate age distributions that differ in their slopes, and thus in their median age. The initial half-lives of *P. tenuisculpta* and *N. taphria* shells in the TAZ are effectively decadal owing to rapid disintegration, comparable to the constant half-life of  $^{210}\text{Pb}$ , and so the large magnitude of offset observed between  $^{210}\text{Pb}$ - and  $^{14}\text{C}$ -based estimates of age likely results from the strong increase in preservational half-life that shells undergo with progressive age and/or burial to the SZ (shift from  $\lambda_1$  to  $\lambda_2$ , Tomašových et al., 2014, 2016). This dynamic emerges from their strongly right-skewed AFD and thus is not restricted to Southern California (Kidwell, 2013). By virtue of their greater durability, shells have longer residence times and can also survive a larger number of postdepositional mixing events than tracers with shorter half-lives. They can thus bear witness to more prolonged and persistent mixing in a sedimentary increment, leading to apparent differences between shells and  $^{210}\text{Pb}$  tracers in estimates both of sedimentation rates and mixing depth. The age homogeneity of *N. taphria* shells in the upper 20–25 cm at both sites clearly indicates that Unit 1 is strongly mixed on a millennial timescale (the age homogeneity of *P. tenuisculpta* shells is probably enhanced by its twentieth century production pulse related to wastewater), just as the age-homogeneous part of the  $^{210}\text{Pb}$  profile indicates that the upper 10–15 cm is completely mixed on a decadal timescale.

Extensive mixing within Unit 1 (including the admixing of shells introduced from deeper units) is also indicated by the strong damping in the core record of a well-documented twentieth century peak in the pollution-tolerant *P. tenuisculpta* (Leonard-Pingel et al., 2019). This species constituted >90% of the living bivalve community near PVL10-50 in the 1970 to 1980s on the basis of annual monitoring data (Figure 11c) but peaked at only 20% at 10–12 cm in both boxcores there. The mild unimodal trajectory of *P. tenuisculpta* in cores reflects both bioadvection within the SML, smearing the stratigraphic distribution of shells produced during the production pulse, and the admixing of much older shells exhumed from below the SML, diluting the pulse. It is quite remarkable that, notwithstanding the 20-cm-thick completely-mixed layer and the extremely low long-term sedimentation rate here, Unit 1 preserves any stratigraphically incremental signal of twentieth century paleoecological history, including both the peak in proportional abundance of *P. tenuisculpta* at 10–12 cm (maximum abundance in the 1980s, Figure 11) and the abundance of *Modiolus* debris at 8–10 cm (Figure 4), reflecting a temporary colonization of the entire Palos Verdes shelf in circa 1985. N.B. that the temporally highly resolved stratigraphies of DDT and other pollutants reported from the Palos Verdes shelf (e.g., Eganhouse & Pontolillo, 2000; Liao et al., 2017; Stull et al., 1996) are based on cores of the effluent layer nearer to the Whites Point outfall, where sedimentation rates were much higher in the late twentieth century and deep burrowers are still recovering from prolonged sediment toxicity and anoxia.

#### 4.2. Within-Species Age Offsets Are Not Fully Explained by SML Thickness

The limited temporal window over which *P. tenuisculpta* achieved high abundance—that is, the major peak in abundance limited to the twentieth century—results in a much smaller IQR of shells ages (age offset) for this species than seen in *N. taphria*. The age offset of *P. tenuisculpta* predicted by sedimentation rate and SML thickness would actually be larger than that observed, because the prediction would assume that production had been constant. For example, under steady-state production and no mixing, a long-term shell burial rate of ~0.005–0.008 cm/year would predict that the IQR of shell ages in each 4-cm increment would be ~550–880 years. Adding mixing within the SML only, the transit time of shells from increments within the 20- to 24-cm-thick SML to deeper increments would be ~2,500–4,000 years, and thus, their expected IQR within the SML would be ~2,700–4,400 years.

In contrast, *N. taphria* has larger age offset per increment within the SML than predicted because its populations were relatively large during most of the late highstand up until the beginning of the twentieth century (Figure 11). The predicted IQR of ~3,300 years corresponds relatively well to the IQRs of *N. taphria* observed

in most of the core at PVL10-50 (2,000–4,000 years), but its IQRs in Unit 1 (SML) at OC-50 are larger (~5,000 years). Similarly, IQRs of *P. tenuisculpta* in Unit 3 achieve ~5,400 years. Mixing over a greater stratigraphic thickness than the SML is thus required. Indeed, the 1,000-year age cohorts of both species are typically distributed over ~40 cm or more of core depth, especially at OC-50 (Figure 9), indicating that burrowers reach well below the 20- to 25-cm-thick SML and thus create the IML. Although it is possible that some inflation in the within-species age offset is generated by horizontal transport of old shells from sediment-starved sites (rather than by deep within-site bioadvection), open burrows located up to 30–40 cm in vibracores are consistent with this inference; moreover, evidence for strong lateral transport of shells across either of these shelves is both lacking and unlikely (the oldest shells are generally at the shelf-slope break, too deep to be mobilized by storms). The reworking upward of shells from the IML thus contributes significantly to the broad stratigraphic distribution of shell cohorts within cores and their extensive age offset per increment within the SML.

Thus, although the scale of within-species temporal resolution in an increment can be predicted to some degree from  $^{14}\text{C}$ -based estimates of sedimentation rates and thickness of the SML, it cannot be accounted for by these two parameters alone. Incomplete mixing extending to ~50 cm, into the SZ and well below the TAZ, and the resulting upward bioadvection of old shells from past production pulses that are preserved in that IML (and/or their retention within the SML), are required. The upward advection is particularly effective because of the higher absolute abundance of shells in the Unit 2 shell bed; those older cohorts (>3,000 years) are most frequent in the shell bed Unit 2 but occur up into Unit 1 (Figure 9). In contrast, the youngest cohorts of both species occur almost exclusively within Unit 1 (with *P. tenuisculpta* shells sourced primarily from twentieth century populations; Figure 9).

#### 4.3. Deep Burrowers That Penetrate Below the TAZ Exhume Very Old Cohorts

Strongly right-skewed, L-shaped AFDs with a mixture of very young cohorts (corresponding to median ages of Unit 1) and cohorts that are 2,000–10,000 years old (corresponding to the median ages typical of Units 2 and 3) occur within each 4-cm increment in Unit 1 (SML; Figure 7). This downcore homogeneity of L-shaped AFDs within Unit 1, with dominance by young cohorts (Figure 7), indicates that shells of both species were rapidly admixed over the entire 20–24 cm of the SML. The absence of these young cohorts in the AFDs of Unit 2 also shows that the SML does not extend down into Unit 2. The young cohorts in Unit 1 were subjected to high, decadal-scale disintegration as evidenced by high values of  $\lambda_1$  (derived from Unit 1 AFDs), showing that this unit at both sites corresponds not only to the SML but also to the TAZ. Therefore, the TAZ and SML coincide in the sediment column. Visual observations of boxcores show that the TAZ encompasses the redox discontinuity between a surficial, light-brownish sediment and a dark-gray subsurface sediment is irregular, occurring at ~5–8 cm at PVL10-50 and at 10 cm at OC-50, with mottled biofabric and oxidized burrows extending to 15–20 cm. This indicates that the TAZ is temporarily exposed to alternating redox oscillations owing to the repeated formation and disappearance of burrows, leading to oxidation of sulfides and ammonia and to carbonate dissolution (Aller, 1982).

The ages of the shells that constitute the tails of the AFDs in Unit 1 correspond to the ages of the most frequent shell age cohorts in Units 2 and 3, suggesting that Units 2 and 3 are the source of those old shells in Unit 1. These deeper units thus most probably represent a SZ for shells, where rates of shell loss were very low, with half-lives comparable to  $\lambda_2$ . Deep burrowers reaching to 40–50 cm, creating an IML, were the most likely mechanism for vertical advection of shells up into Unit 1. The TAZ thus extended only to the base of the SML, but burrowing extended down into the SZ. Therefore, the upper part of the SZ coincides with the IML, and the maximum depth of bioadvection (IML) and the depth of high shell disintegration rates (TAZ) are thus decoupled.

The preservation of carbonate shells on the Southern California shelf thus follows a sequestration-exhumation dynamic where the depth of maximum bioturbation exceeds the depth of the TAZ (Figure 12a). Under this dynamic, the traditional subdivision of sediments according to bioturbational mixing into a completely-mixed surface layer and an incompletely-mixed subsurface layer (SML and IML here) is, here, tightly coupled with the transition from a taphonomically distinct high-loss TAZ to a lower-loss SZ. Shells buried below the SML (and TAZ) attain a refuge, within the IML, from high disintegration rates, allowing them to accumulate. This refuge might only be temporary: Shells are still subject to possible reworking back into the TAZ. This model would explain the stratigraphic record at both of our coring sites, separated by ~26 km.

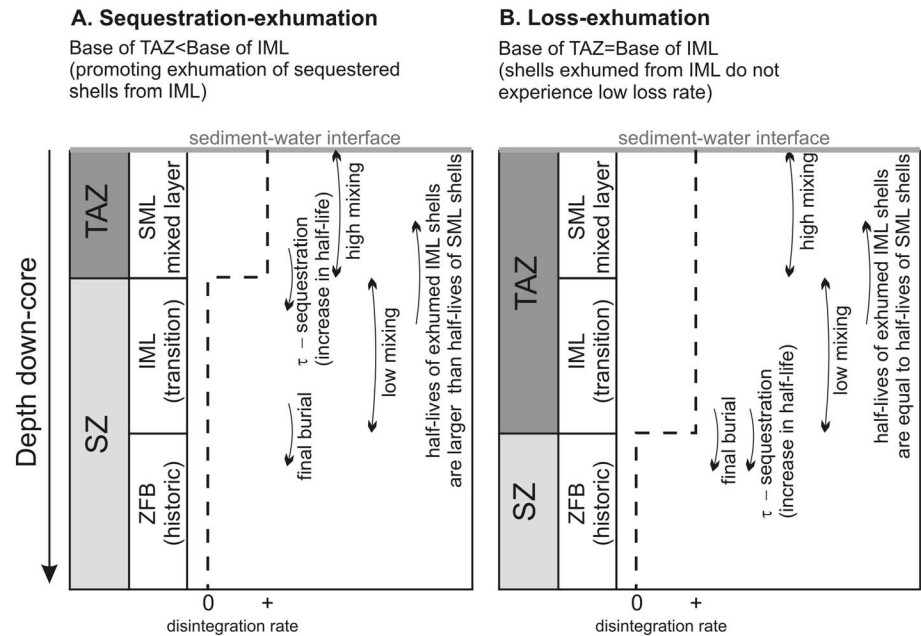


**Figure 12.** Two alternate relationships between the depth of the TAZ (taphonomic active zone, where loss rates from dissolution and microbial disintegration are high) and the depth of sediment mixing induced by bioturbation, affecting the potential for strong age offsets among shells in surficial sediments. Bioturbational mixing depth and frequency are envisaged as declining with depth below the sediment-water interface, generating a three-layer model, with a surface completely mixed layer (SML), a subsurface incompletely-mixed layer (IML), and a layer without any active mixing (i.e., historic layer or zone of final burial, ZFB). The TAZ denotes the sediment increment where loss rates are very high, contrasting with the sequestration zone (SZ) where loss rates of resident shells are low. In the sequestration-exhumation scenario (a), characterizing settings with relatively low sedimentation rate and/or deep burrowing, the depth of the TAZ is shallower than the depth of the IML, and thus, shells that are exhumed from the sequestration zone (SZ) into the TAZ can be significantly older than shells that have remained within the TAZ. In the loss-exhumation scenario (b), characterizing settings of high sedimentation or only shallow burrowing, the depth of the TAZ coincides with the depth of the IML. Cohorts of older shells have thus been subject to consistently high loss rates, the same as young cohorts, rather than benefiting from temporary sequestration: shells from old cohorts do not accumulate preferentially in the IML, and thus their exhumation up into the SML is less likely to affect the age-frequency distribution within the SML than in the sequestration-exhumation scenario.

An alternative scenario—characterized by a loss-exhumation dynamic—might apply in settings with higher sedimentation rate (e.g., estuaries, lagoons, and deltas and late highstand shelves) or shallower bioturbation in oxygen limited environments. Where the depth of maximum sediment mixing induced by bioturbation does not exceed the depth of the TAZ, then both the SML and the IML lie within the TAZ (Figure 12b). All shells affected by upward and downward mixing would thus be subject to the same high taphonomic loss, prohibiting the accumulation of old shells within the reach of bioturbation.

#### 4.4. Between-Species Age Offsets Result From Their Out-of-Phase Production

In Southern California, biomonitoring in the late twentieth century provides empirical confirmation of the results of our age unmixing of core assemblages, namely, that shell production of our two species were out of phase, with a recent outbreak in *P. tenuisculpta* and a decline in *N. taphria*. *P. tenuisculpta* is moderately tolerant to sediment pollution (Ferraro et al., 1991). Its populations exploded in the 1970s and declined to very low levels over the late 1980s and 1990s. In contrast, *N. taphria* prefers sandy substrates and is sensitive to sediment pollution (Smith et al., 2001; Zmarzly et al., 1994). It was reported as frequent on the San Pedro shelf in the 1950s but disappeared in the late twentieth century and has been scarce for that entire interval on the Palos Verdes shelf (Figure 11).

The between-species age offsets observed in Unit 1 and in Unit 3 thus result from these differences in production that were driven by differences in their substrate requirements and sensitivity to organic

enrichment and pollution. The lack or rarity of *P. tenuisculpta* shells during the highstand phase strongly limits the scale of age offset within that species in Unit 1. In contrast, the lack of young *N. taphria* shells and the abundance of old ones available for exhumation from the SZ Units 2 and 3 result in larger IQRs and an older median shell age in Unit 1. Finally, the transgressive peak in abundance of *P. tenuisculpta* (~10,000–12,000 years ago), preceding the timing of maximum abundance of *N. taphria*, generates the age offset in Unit 3. The net effect is millennial-scale age offset of two cooccurring species within Units 1 and 3.

Raw stratigraphic patterns in species abundances detect the recentmost increase in *P. tenuisculpta* production but not the recentmost decline of *N. taphria* (Figures 10 and 11). Due to the upward advection of abundant older *N. taphria* shells from the subsurface shell-rich units that represent the SZ up into Unit 1, the stratigraphic signal of their recentmost population decline recovered by age unmixing is lost. Similarly, the gradual increase in production of *N. taphria* through the late-transgressive phase toward the highstand phase is smeared by the downward advection of shells to the base of Unit 3 (Figure 10a). Without the offsets in production, combined with the condition of the IML extending below the TAZ, the age offsets between these two cooccurring species would be insignificant. Assuming that all species had temporally constant production, or had synchronized changes in production, is unrealistic of course, under both natural and anthropogenic environmental change and when individual species differ in their ecological requirements. Between-species age offsets as documented here in Holocene Units 1 and 3 of the Southern California shelf have been also observed in other settings (Kosnik et al., 2009, 2013; Tomašových et al., 2019) and can be expected to be especially common in environments with moderate to low sedimentation and substantial bioturbation.

#### Acknowledgments

All data are deposited at doi.pangaea.de/10.1594/PANGAEA.900879. Cores were acquired during cruise MV1211 of the RV Melville out of the University of California San Diego. For field assistance we thank the crew; undergraduate and graduate student volunteers from the University of Chicago, Savannah State University, and UCSD; and professional volunteers T. Parker and C. MacDonald (LACSD), B. Edwards (USGS), R. Cipriani (Santa Monica), and J. McNinch and H. Wadman (USACE), who provided crucial vibracore equipment. For field and lab assistance we thank L. DeLeo, M. Robinson, and C. Venherm (Skidaway) and J. Leonard-Pingel (Ohio State University); and for lab assistance Katherine Whitacre (NAU). For access to historical data on living bivalves of the Palos Verdes and San Pedro shelves and biological insights, we are grateful to the Sanitation Districts of Los Angeles County and the Orange County Sanitation District, particularly D. Cadien, W. Powers, and K. Barwick for facilitating approval. We thank two reviewers for helpful reviews of the manuscript. Research supported by NSF EAR-112418 (S. K. and A. T.) and 1124318 (CA), with pilot work supported by a National Oceanic and Atmospheric Association Sea Grant administered by the University of Southern California (NA07OAR417 0008), by the Slovak Research and Development Agency (APVV17-0555), and the Slovak Scientific Grant Agency (VEGA 0169/19).

#### 5. Conclusions

Downcore changes in median shell age indicate that (1) long-term sedimentation rates at these sites were slow (~0.005 cm/year); (2) the 20- to 25-cm-thick SML coincides with the TAZ, given that shell age distributions are homogeneous within the entirety of Unit 1 and are dominated by young cohorts (and thus reflecting high disintegration rates); and (3) bioturbation to depths of 40–50 cm (the IML) allowed the exhumation of significantly older shells from subsurface SZs (Units 2 and 3) back up into Unit 1 (the SML and TAZ). The differences in the ages of shells of cooccurring species within Units 1 and 3 cannot be explained by differences in their disintegration rates, in contrast to the Barker Effect of Broecker and Clark (2011): The AFDs of both species indicate that they both experienced the same initially high disintegration rates, with decadal taphonomic half-lives. Instead, between-species age offsets within the SML are explained by out-of-phase production of these two species. Thus, significant age offsets are generated under the relatively slow sedimentation rates and deep bioturbation typical of continental shelves, smearing and attenuating the stratigraphic record of temporal changes in species abundances. The thickness of the SML alone, such as used in most deconvolution models, cannot explain observed age offsets within species in fossil assemblages, and out-of-phase changes in production are required to explain age offsets between species.

#### References

- Alegret, L., Rodríguez-Tovar, F. J., & Uchman, A. (2015). How bioturbation obscured the Cretaceous–Palaeogene boundary record. *Terra Nova*, 27, 225–230.
- Alexander, C. R., & Lee, H. J. (2009). Sediment accumulation on the Southern California Bight continental margin during the twentieth century. *Geological Society of America Special Papers*, 454, 69–87.
- Allan Hancock Foundation (1965). *An oceanographic and biological survey of the southern California mainland shelf*, (Vol. 27, pp. 1–232). California: State Water Quality Control Board, Publication.
- Allen, A. P., Kosnik, M. A., & Kaufman, D. S. (2013). Characterizing the dynamics of amino acid racemization using time-dependent reaction kinetics: A Bayesian approach to fitting age-calibration models. *Quaternary Geochronology*, 18, 63–77.
- Aller, R. C. (1982). Carbonate dissolution in nearshore terrigenous muds: The role of physical and biological reworking. *Journal of Geology*, 90, 79–95.
- Aller, R. C. (1994). Bioturbation and remineralization of sedimentary organic matter: Effects of redox oscillation. *Chemical Geology*, 114, 331–345.
- Anderson, D. M. (2001). Attenuation of millennial-scale events by bioturbation in marine sediments. *Paleoceanography*, 16, 352–357.
- Anderson, J. W., Reish, D. J., Spies, R. B., Brady, M. E., & Segelhorst, E. W. (1993). *Human impacts. Ecology of the Southern California Bight: a Synthesis and Interpretation*, (pp. 682–766). Los Angeles, CA: University of California Press.

- Anderson, L. C., Sen Gupta, B. K., McBride, R. A., & Byrnes, M. R. (1997). Reduced seasonality of Holocene climate and pervasive mixing of Holocene marine section: Northeastern Gulf of Mexico shelf. *Geology*, *25*, 127–130.
- Ausin, B., Haghypour, N., Wacker, L., Voelker, A. H., Hodell, D., Magill, C., et al. (2019). Radiocarbon age offsets between two surface dwelling planktonic foraminifera species during abrupt climate events in the SW Iberian margin. *Paleoceanography and Paleoclimatology*, *34*, 63–78. <https://doi.org/10.1029/2018PA003490>
- Bard, E. (2001). Paleoceanographic implications of the difference in deep-sea sediment mixing between large and fine particles. *Paleoceanography and Paleoclimatology*, *16*, 235–239.
- Bard, E., Arnold, M., Duprat, J., Moyes, J., & Duplessy, J. C. (1987). Reconstruction of the last deglaciation: Deconvolved records of  $\delta^{18}\text{O}$  profiles, micropaleontological variations and accelerator mass spectrometric  $^{14}\text{C}$  dating. *Climate Dynamics*, (2), 101–112.
- Barker, S., Broecker, W., Clark, E., & Hajdas, I. (2007). Radiocarbon age offsets of foraminifera resulting from differential dissolution and fragmentation within the sedimentary bioturbated layer. *Paleoceanography*, *22*, PA2205. <https://doi.org/10.1029/2006PA001354>
- Bentley, S. J., & Nittrouer, C. A. (2003). Emplacement, modification, and preservation of event strata on a flood-dominated continental shelf: Eel shelf, Northern California. *Continental Shelf Research*, *23*, 1465–1493.
- Bentley, S. J., & Nittrouer, C. A. (2012). Accumulation and intense bioturbation of bioclastic muds along a carbonate-platform margin: Dry Tortugas, Florida. *Marine Geology*, *315*, 44–57.
- Bentley, S. J., Sheremet, A., & Jaeger, J. M. (2006). Event sedimentation, bioturbation, and preserved sedimentary fabric: Field and model comparisons in three contrasting marine settings. *Continental Shelf Research*, *26*, 2108–2124.
- Berger, W. H., Ekdale, A. A., & Bryant, P. P. (1979). Selective preservation of burrows in deep-sea carbonates. *Marine Geology*, *32*, 205–230.
- Birks, C. J., & Koç, N. (2002). A high-resolution diatom record of late Quaternary sea-surface temperatures and oceanographic conditions from the eastern Norwegian Sea. *Boreas*, *31*, 323–344.
- Broecker, W., & Clark, E. (2011). Radiocarbon age differences among coexisting planktic foraminifera shells: The Barker effect. *Paleoceanography*, *26*, PA2222. <https://doi.org/10.1029/2011PA002116>
- Broecker, W. S., Klas, M., & Clark, E. (1991). The influence of  $\text{CaCO}_3$  dissolution on the core top radiocarbon ages for deep sea sediments. *Paleoceanography*, *6*, 593–608.
- Broecker, W. S., Matsumoto, K., Clark, E., Hajdas, I., & Bonani, G. (1999). Radiocarbon age differences between coexisting foraminiferal species. *Paleoceanography*, *14*, 431–436.
- Cherns, L., & Wright, V. P. (2011). Skeletal mineralogy and biodiversity of marine invertebrates: size matters more than seawater chemistry. *Geological Society Special Publication*, *358*, 9–17.
- Davies, D. J., Powell, E. N., & Stanton, R. J. Jr. (1989). Relative rates of shell dissolution and net sediment accumulation—a commentary: Can shell beds form by the gradual accumulation of biogenic debris on the sea floor? *Lethaia*, *22*, 207–212.
- Diener, D. R., Fuller, S. C., Lissner, A., Haydock, C. I., Maurer, D., Robertson, G., & Gerlinger, T. (1995). Spatial and temporal patterns of the infaunal community near a major ocean outfall in Southern California. *Marine Pollution Bulletin*, *30*, 861–878.
- Dominguez, J. G., Kosnik, M. A., Allen, A. P., Hua, Q., Jacob, D. E., Kaufman, D. S., & Whitacre, K. (2016). Time-averaging and stratigraphic resolution in death assemblages and Holocene deposits: Sydney Harbour's molluscan record. *Palaios*, *31*, 563–574.
- DuBois, L. G., & Prell, W. L. (1988). Effects of carbonate dissolution on the radiocarbon age structure of sediment mixed layers. *Deep Sea Research Part A. Oceanographic Research Papers*, *35*, 1875–1885.
- Eganhouse, R. P., & Pontolillo, J. (2000). Depositional history of organic contaminants on the Palos Verdes Shelf, California. *Marine Chemistry*, *70*, 317–338.
- Ekdale, A. A., Muller, L. N., & Novak, M. T. (1984). Quantitative ichnology of modern pelagic deposits in the abyssal Atlantic. *Palaeogeography, Palaeoclimatology, Palaeoecology*, *45*, 189–223.
- Emery, K. O. (1952). Continental shelf sediments of Southern California. *Geological Society of America Bulletin*, *63*, 1105–1108.
- Fabrikant, R. (1984). The effect of sewage effluent on the population density and size of the clam *Parvilucina tenuisculpta*. *Marine Pollution Bulletin*, *15*, 249–253.
- Ferraro, S. P., Swartz, R. C., Cole, F. A., & Schults, D. W. (1991). Temporal changes in the benthos along a pollution gradient: Discriminating the effect of natural phenomena from sewage-industrial wastewater effects. *Estuarine, Coastal and Shelf Science*, *33*, 383–407.
- Ferré, B., Sherwood, C. R., & Wiberg, P. L. (2010). Sediment transport on the Palos Verdes shelf, California. *Continental Shelf Research*, *30*, 761–780.
- Fisher, M. A., Normark, W. R., Langenheim, V. E., Calvert, A. J., & Sliter, R. (2004). The Offshore Palos Verdes Fault Zone near San Pedro, Southern California. *Bulletin of the Seismological Society of America*, *94*, 506–530.
- Guinasso, N. L., & Schink, D. R. (1975). Quantitative estimates of biological mixing rates in abyssal sediments. *Journal of Geophysical Research*, *80*, 3032–3043.
- Hartmann, O. (1966). *Quantitative survey of the benthos of San Pedro Basin, southern California. Part II. Final results and conclusions*, (Vol. 19, p. 459). Los Angeles, CA: University of Southern California, Allan Hancock Foundation Pacific Expeditions.
- Henderson, G. M., Lindsay, F. N., & Slowey, N. C. (1999). Variation in bioturbation with water depth on marine slopes: A study on the Little Bahamas Bank. *Marine Geology*, *160*, 105–118.
- Hendy, I. L., Dunn, L., Schimmelmann, A., & Pak, D. K. (2013). Resolving varve and radiocarbon chronology differences during the last 2000 years in the Santa Barbara Basin sedimentary record, California. *Quaternary International*, *310*, 155–168.
- Hull, P. M., Franks, P. J., & Norris, R. D. (2011). Mechanisms and models of iridium anomaly shape across the Cretaceous–Paleogene boundary. *Earth and Planetary Science Letters*, *301*, 98–106.
- Johannessen, S. C., & Macdonald, R. W. (2012). There is no 1954 in that core! Interpreting sedimentation rates and contaminant trends in marine sediment cores. *Marine Pollution Bulletin*, *64*, 675–678.
- Jones, G. F. (1969). *The benthic macrofauna of the mainland shelf of Southern California*, Allan Hancock Monographs in Marine Biology, (Vol. 4, pp. 1–219).
- Kaufman, D. S., & Manley, W. F. (1998). A new procedure for determining dl amino acid ratios in fossils using reverse phase liquid chromatography. *Quaternary Science Reviews*, *17*, 987–1000.
- Keigwin, L. D., & Guilderson, T. P. (2009). Bioturbation artifacts in zero-age sediments. *Paleoceanography*, *24*, PA4212. <https://doi.org/10.1029/2008PA001727>
- Keigwin, L. D., & Jones, G. A. (1995). The marine record of deglaciation from the continental margin off Nova Scotia. *Paleoceanography*, *10*, 973–985.
- Kemp, D. B., & Sexton, P. F. (2014). Time-scale uncertainty of abrupt events in the geologic record arising from unsteady sedimentation. *Geology*, *42*, 891–894.

- Kidwell, S. M. (2013). Time-averaging and fidelity of modern death assemblages: Building a taphonomic foundation for conservation palaeobiology. *Palaeontology*, *56*, 487–522.
- Knies, J., Hald, M., Ebbesen, H., Mann, U., & Vogt, C. (2003). A deglacial–middle Holocene record of biogenic sedimentation and paleo-productivity changes from the northern Norwegian continental shelf. *Paleoceanography*, *18*(4), 1096. <https://doi.org/10.1029/2002PA000872>
- Kobashi, T., Grossman, E. L., Dockery, D. T., & Ivany, L. C. (2004). Water mass stability reconstructions from greenhouse (Eocene) to icehouse (Oligocene) for the northern Gulf Coast continental shelf (USA). *Paleoceanography*, *19*, PA1022. <https://doi.org/10.1029/2003PA000934>
- Kosnik, M. A., Hua, Q., Jacobsen, G. E., Kaufman, D. S., & Wüst, R. A. (2007). Sediment mixing and stratigraphic disorder revealed by the age-structure of *Tellina* shells in Great Barrier Reef sediment. *Geology*, *35*, 811–814.
- Kosnik, M. A., Hua, Q., Kaufman, D. S., & Wüst, R. A. (2009). Taphonomic bias and time-averaging in tropical molluscan death assemblages: Differential shell half-lives in Great Barrier Reef sediment. *Paleobiology*, *35*, 565–586.
- Kosnik, M. A., Hua, Q., Kaufman, D. S., & Zawadzki, A. (2015). Sediment accumulation, stratigraphic order, and the extent of time-averaging in lagoonal sediments: a comparison of <sup>210</sup>Pb and <sup>14</sup>C/amino acid racemization chronologies. *Coral Reefs*, *34*, 215–229.
- Kosnik, M. A., & Kaufman, D. S. (2008). Identifying outliers and assessing the accuracy of amino acid racemization measurements for geochronology: II. Data screening. *Quaternary Geochronology*, *3*, 328–341.
- Kosnik, M. A., Kaufman, D. S., & Hua, Q. (2013). Radiocarbon-calibrated multiple amino acid geochronology of Holocene molluscs from Bramble and Rib Reefs (Great Barrier Reef, Australia). *Quaternary Geochronology*, *16*, 73–86.
- Kristensen, E. (2000). Organic matter diagenesis at the oxic/anoxic interface in coastal marine sediments, with emphasis on the role of burrowing animals. *Hydrobiologia*, *426*, 1–24.
- Kuzyk, Z. Z. A., Macdonald, R. W., & Johannessen, S. C. (2015). Calculating rates and dates and interpreting contaminant profiles in bioturbated sediments. In J. M. Blais (Ed.), *Environmental Contaminants*, (pp. 61–87). Dordrecht: Springer Science. [https://doi.org/10.1007/978-94-017-9541-8\\_4](https://doi.org/10.1007/978-94-017-9541-8_4)
- Lazarus, D., Weinkauff, M., & Diver, P. (2012). Pacman profiling: a simple procedure to identify stratigraphic outliers in high-density deep-sea microfossil data. *Paleobiology*, *38*, 144–161.
- Lee, H. J., Sherwood, C. R., Drake, D. E., Edwards, B. D., Wong, F., & Hamer, M. (2002). Spatial and temporal distribution of contaminated, effluent-affected sediment on the Palos Verdes margin, southern California. *Continental Shelf Research*, *22*, 859–880.
- Leonard-Pingel, J. S., Kidwell, S. M., Tomašových, A., Alexander, C. R., & Cadien, D. B. (2019). Gauging benthic recovery from 20<sup>th</sup> century pollution on the southern California continental shelf using bivalves from sediment cores. *Marine Ecology Progress Series*, *615*, 101–119.
- Liao, C., Taylor, A. R., Kenney, W. F., Schlenk, D., & Gan, J. (2017). Historical record and fluxes of DDTs at the Palos Verdes Shelf Superfund site, California. *Science of the Total Environment*, *581*, 697–704.
- Loubere, P. (1989). Bioturbation and sedimentation rate control of benthic microfossil taxon abundances in surface sediments: A theoretical approach to the analysis of species microhabitats. *Marine Micropaleontology*, *14*, 317–325.
- Löwemark, L. (2007). Importance and usefulness of trace fossils and bioturbation in paleoceanography. In W. Miller, III (Ed.), *Trace Fossils*, (pp. 413–427). Amsterdam: Elsevier Science.
- Löwemark, L., & Grootes, P. M. (2004). Large age differences between planktic foraminifers caused by abundance variations and *Zoophycos* bioturbation. *Paleoceanography*, *19*, PA2001. <https://doi.org/10.1029/2003PA000949>
- MacLeod, K. G., & Huber, B. T. (1996). Strontium isotopic evidence for extensive reworking in sediments spanning the Cretaceous-Tertiary boundary at ODP Site 738. *Geology*, *24*, 463–466.
- Maire, O., Lecroart, P., Meysman, F., Rosenberg, R., Duchêne, J. C., & Grémare, A. (2008). Quantification of sediment reworking rates in bioturbation research: A review. *Aquatic Biology*, *2*, 219–238.
- Manighetti, B., McCave, I. N., Maslin, M., & Shackleton, N. J. (1995). Chronology for climate change: developing age models for the Biogeochemical Ocean Flux Study cores. *Paleoceanography*, *10*, 513–525.
- Maurer, D., Nguyen, H., Robertson, G., & Gerlinger, T. (1999). The Infaunal Trophic Index (ITI): its suitability for marine environmental monitoring. *Ecological Applications*, *9*, 699–713.
- Maurer, D., Robertson, G., & Gerlinger, T. (1993). Long-term temporal and spatial fluctuations of soft bottom infaunal invertebrates associated with an ocean outfall from the San Pedro shelf, California. *International Review of Hydrobiology*, *78*, 535–555.
- McCave, I. N. (1988). Biological pumping upwards of the coarse fraction of deep-sea sediments. *Journal of Sedimentary Research*, *58*, 148–158.
- McNeilan, T. W., Rockwell, T. K., & Resnick, G. S. (1996). Style and rate of Holocene slip, Palos Verdes fault, southern California. *Journal of Geophysical Research*, *101*, 8317–8334.
- Mekik, F. (2014). Radiocarbon dating of planktonic foraminifer shells: A cautionary tale. *Paleoceanography and Paleoclimatology*, *29*, 13–29.
- Meysman, F. J., Boudreau, B. P., & Middelburg, J. J. (2010). When and why does bioturbation lead to diffusive mixing? *Journal of Marine Research*, *68*, 881–920.
- Myhre, S. E., Kroeker, K. J., Hill, T. M., Roopnarine, P., & Kennett, J. P. (2017). Community benthic paleoecology from high-resolution climate records: Mollusca and Foraminifera in post-glacial environments of the California Margin. *Quaternary Science Reviews*, *155*, 179–197.
- Nardin, T. R. (1983). Late Quaternary depositional systems and sea level change, Santa Monica and San Pedro Basins, California continental borderland. *American Association of Petroleum Geologists Bulletin*, *67*, 1104–1124.
- Nardin, T. R., & Henyey, T. L. (1978). Pliocene-Pleistocene diastrophism of Santa Monica and San Pedro shelves, California continental borderland. *AAPG Bulletin*, *62*, 247–272.
- Nardin, T. R., Osborne, R. H., Bottjer, D. J., & Scheidemann, R. C. (1981). Holocene sea-level curves for Santa Monica shelf, California continental borderland. *Science*, *213*, 331–333.
- Nawrot, R., Scarponi, D., Azzarone, M., Dexter, T. A., Kusnerik, K. M., Wittmer, J. M., et al. (2018). Stratigraphic signatures of mass extinctions: Ecological and sedimentary determinants. *Proceedings of the Royal Society of London*, *B285*, 20181191.
- Niedoroda, A. W., Swift, D. J., Reed, C. W., & Stull, J. K. (1996). Contaminant dispersal on the Palos Verdes continental margin: III. Processes controlling transport, accumulation and re-emergence of DDT-contaminated sediment particles. *Science of the Total Environment*, *179*, 109–133.
- O’Dea, A., Jackson, J. B., Fortunato, H., Smith, J. T., D’Croz, L., Johnson, K. G., & Todd, J. A. (2007). Environmental change preceded Caribbean extinction by 2 million years. *Proceedings of the National Academy of Sciences*, *104*, 5501–5506.

- Olszewski, T. D. (2004). Modeling the influence of taphonomic destruction, reworking, and burial on time-averaging in fossil accumulations. *Palaios*, *19*, 39–50.
- Olszewski, T. D., & Kaufman, D. S. (2015). Tracing burial history and sediment recycling in a shallow estuarine setting (Copano Bay, Texas) using postmortem ages of the bivalve *Mulinia lateralis*. *Palaios*, *30*, 224–237.
- Pandolfi, J. M. (1996). Limited membership in Pleistocene reef coral assemblages from the Huon Peninsula, Papua New Guinea: Constancy during global change. *Paleobiology*, *22*, 152–176.
- Paola, C., Ganti, V., Mohrig, D., Runkel, A. C., & Straub, K. M. (2018). Time not our time: Physical controls on the preservation and measurement of geologic time. *Annual Review of Earth and Planetary Sciences*, *46*(1), 409–438. <https://doi.org/10.1146/annurev-earth-082517-010129>
- Paull, C. K., Hills, S. J., Thierstein, H. R., Bonani, G., & Wöflfi, W. (1991).  $^{14}\text{C}$  offsets and apparently non-synchronous  $\delta^{18}\text{O}$  stratigraphies between nannofossil and foraminiferal pelagic carbonates. *Quaternary Research*, *35*, 274–290.
- Peng, T. H., & Broecker, W. S. (1984). The impacts of bioturbation on the age difference between benthic and planktonic foraminifera in deep sea sediments. *Nuclear Instruments and Methods in Physics Research Section B*, *233*, 346–352.
- Peng, T. H., Broecker, W. S., & Berger, W. H. (1979). Rates of benthic mixing in deep-sea sediment as determined by radioactive tracers. *Quaternary Research*, *11*(1), 141–149. [https://doi.org/10.1016/0033-5894\(79\)90074-7](https://doi.org/10.1016/0033-5894(79)90074-7)
- Reimer, P. J., Bard, E., Bayliss, A., Beck, J. W., Blackwell, P. G., Ramsey, C. B., et al. (2013). IntCal13 and Marine13 radiocarbon age calibration curves 0–50,000 years cal BP. *Radiocarbon*, *55*, 1869–1887.
- Ritter, M. D. N., Erthal, F., Kosnik, M. A., Coimbra, J. C., & Kaufman, D. S. (2017). Spatial variation in the temporal resolution of subtropical shallow-water molluscan death assemblages. *Palaios*, *32*, 572–583.
- Sadler, P. M. (1981). Sediment accumulation rates and the completeness of stratigraphic sections. *Journal of Geology*, *89*, 569–584.
- Sanchez-Cabeza, J. A., & Ruiz-Fernández, A. C. (2012).  $^{210}\text{Pb}$  sediment radiochronology: An integrated formulation and classification of dating models. *Geochimica et Cosmochimica Acta*, *82*, 183–200. <https://doi.org/10.1016/j.gca.2010.12.024>
- Santschi, P. H., Guo, L., Asbill, S., Allison, M., Kepple, A. B., & Wen, L. S. (2001). Accumulation rates and sources of sediments and organic carbon on the Palos Verdes shelf based on radioisotopic tracers ( $^{137}\text{Cs}$ ,  $^{239,240}\text{Pu}$ ,  $^{210}\text{Pb}$ ,  $^{234}\text{Th}$ ,  $^{238}\text{U}$  and  $^{14}\text{C}$ ). *Marine Chemistry*, *73*, 125–152.
- Savrda, C. E., Bottjer, D. J., & Seilacher, A. (1991). Redox-related benthic events. In G. Einsele, W. Ricken, & A. Seilacher (Eds.), *Cycles and Events in Stratigraphy*, (pp. 524–528). Berlin: Springer-Verlag.
- Scarponi, D., Kaufman, D., Amorosi, A., & Kowalewski, M. (2013). Sequence stratigraphy and the resolution of the fossil record. *Geology*, *41*, 239–242.
- Schiffelbein, P. (1985). Extracting the benthic mixing impulse response function: A constrained deconvolution technique. *Marine Geology*, *64*, 313–336.
- Schiffers, K., Teal, L. R., Travis, J. M. J., & Solan, M. (2011). An open source simulation model for soil and sediment bioturbation. *PLoS ONE*, *6*, e28028.
- Schumer, R., Jerolmack, D., & McElroy, B. (2011). The stratigraphic filter and bias in measurement of geologic rates. *Geophysical Research Letters*, *38*, L11405. <https://doi.org/10.1029/2011GL047118>
- Shull, D. H. (2001). Transition-matrix model of bioturbation and radionuclide diagenesis. *Limnology and Oceanography*, *46*, 905–916.
- Smith, C. R., Pope, R. H., DeMaster, D. J., & Magaard, L. (1993). Age-dependent mixing of deep-sea sediments. *Geochimica et Cosmochimica Acta*, *57*, 1473–1488.
- Smith, G. B. (1974). Some effects of sewage discharge to the marine environment. *Doctoral dissertation, University of California, San Diego*, 1–334.
- Smith, R. W., Bergen, M., Weisberg, S. B., Cadien, D., Dalkey, A., Montagne, D., et al. (2001). Benthic response index for assessing infaunal communities on the southern California mainland shelf. *Ecological Applications*, *11*, 1073–1087.
- Sommerfield, C. K., Lee, H. J., & Normark, W. R. (2009). Postglacial sedimentary record of the Southern California continental shelf and slope, Point Conception to Dana Point. *Geological Society of America Special Papers*, *454*, 89–115.
- Stein, E. D., & Cadien, D. B. (2009). Ecosystem response to regulatory and management actions: The southern California experience in long-term monitoring. *Marine Pollution Bulletin*, *59*(4–7), 91–100. <https://doi.org/10.1016/j.marpolbul.2009.02.025>
- Steiner, Z., Lazar, B., Levi, S., Tsroya, S., Pelled, O., Bookman, R., & Erez, J. (2016). The effect of bioturbation in pelagic sediments: Lessons from radioactive tracers and planktonic foraminifera in the Gulf of Aqaba, Red Sea. *Geochimica et Cosmochimica Acta*, *194*, 139–152.
- Stuiver, M., & Reimer, P. J. (1993). Extended  $^{14}\text{C}$  data base and revised CALIB 3.0  $^{14}\text{C}$  age calibration program. *Radiocarbon*, *35*, 215–230.
- Stull, J. K. (1995). Two decades of marine biological monitoring, Palos Verdes, California, 1972 to 1992. *Bulletin of the Southern California Academy of Sciences*, *94*, 21–45.
- Stull, J. K., Haydock, C. I., Smith, R. W., & Montagne, D. E. (1986). Long-term changes in the benthic community on the coastal shelf of Palos Verdes, Southern California. *Marine Biology*, *91*, 539–511.
- Stull, J. K., Swift, D. J., & Niedoroda, A. W. (1996). Contaminant dispersal on the Palos Verdes continental margin: I. Sediments and biota near a major California wastewater discharge. *Science of the Total Environment*, *179*, 73–90.
- Swift, D. J., Stull, J. K., Niedoroda, A. W., Reed, C. W., & Wong, G. T. (1996). Contaminant dispersal on the Palos Verdes continental margin II. Estimates of the biodiffusion coefficient,  $D_B$ , from composition of the benthic infaunal community. *Science of the Total Environment*, *179*, 91–107.
- Teal, L. R., Bulling, M. T., Parker, E. R., & Solan, M. (2008). Global patterns of bioturbation intensity and mixed depth of marine soft sediments. *Aquatic Biology*, *2*, 207–218.
- Thomson, J., Brown, L., Nixon, S., Cook, G. T., & MacKenzie, A. B. (2000). Bioturbation and Holocene sediment accumulation fluxes in the north-east Atlantic Ocean (Benthic Boundary Layer experiment sites). *Marine Geology*, *169*, 21–39.
- Thomson, J., Cook, G. T., Anderson, R., Mackenzie, A. B., Harkness, D. D., & McCave, I. (1995). Radiocarbon age offsets in different-sized carbonate components of deep-sea sediments. *Radiocarbon*, *37*, 91–101.
- Tomašových, A., Gallmetzer, I., Haselmair, A., Kaufman, D., Kralj, M., Cassin, D., et al. (2018). Tracing the effects of eutrophication on molluscan communities in sediment cores: outbreaks of an opportunistic species coincide with reduced bioturbation and high frequency of hypoxia in the Adriatic Sea. *Paleobiology*, *44*, 575–602.
- Tomašových, A., Gallmetzer, I., Haselmair, A., Kaufman, D. S., Mavrič, B., & Zuschin, M. (2019). A decline in molluscan carbonate production driven by the loss of vegetated habitats encoded in the Holocene sedimentary record of the Gulf of Trieste. *Sedimentology*, *66*, 781–807.

- Tomašových, A., Gallmetzer, I., Haselmair, A., Kaufman, D. S., Vidović, J., & Zuschin, M. (2017). Stratigraphic unmixing reveals repeated hypoxia events over the past 500 yr in the northern Adriatic Sea. *Geology*, *45*, 363–366.
- Tomašových, A., & Kidwell, S. M. (2010). The effects of temporal resolution on species turnover and on testing metacommunity models. *American Naturalist*, *175*, 587–606.
- Tomašových, A., & Kidwell, S. M. (2017). Nineteenth-century collapse of a benthic marine ecosystem on the open continental shelf. *Proceedings of the Royal Society of London*, *B284*, 20170328.
- Tomašových, A., Kidwell, S. M., & Barber, R. F. (2016). Inferring skeletal production from time-averaged assemblages: skeletal loss pulls the timing of production pulses towards the modern period. *Paleobiology*, *42*, 54–76.
- Tomašových, A., Kidwell, S. M., Barber, R. F., & Kaufman, D. S. (2014). Long-term accumulation of carbonate shells reflects a 100-fold drop in loss rate. *Geology*, *42*, 819–822.
- Trauth, M. H. (1998). Turbo: a dynamic-probabilistic simulation to study the effects of bioturbation on paleoceanographic time series. *Computers and Geosciences*, *24*, 433–441.
- Uchman, A., & Wetzel, A. (2011). Deep-sea ichnology: The relationships between depositional environment and endobenthic organisms. *Developments in Sedimentology*, *63*, 517–556.
- Wheatcroft, R. A. (1990). Preservation potential of sedimentary event layers. *Geology*, *18*, 843–845.
- Wheatcroft, R. A. (1992). Experimental tests for particle size-dependent bioturbation in the deep ocean. *Limnology and Oceanography*, *37*, 90–104.
- Wheatcroft, R. A., & Drake, D. E. (2003). Post-depositional alteration and preservation of sedimentary event layers on continental margins. I. The role of episodic sedimentation. *Marine Geology*, *199*, 123–137.
- Wit, J. C., Reichart, G. J., & Ganssen, G. M. (2013). Unmixing of stable isotope signals using single specimen  $\delta^{18}\text{O}$  analyses. *Geochemistry, Geophysics, Geosystems*, *14*, 1312–1320. <https://doi.org/10.1002/ggge.20101>
- Zmarzly, D. L., Stebbins, T. D., Pasko, D., Duggan, R. M., & Barwick, K. L. (1994). Spatial patterns and temporal succession in soft-bottom macroinvertebrate assemblages surrounding an ocean outfall on the southern San Diego shelf: Relation to anthropogenic and natural events. *Marine Biology*, *118*, 293–307.

## Erratum

In the originally published version of this paper, there were errors in Figure 12. These errors have since been corrected and this version may be considered the authoritative version of record.